Microwave detector

Document status and date:
Published: 01/01/2014

Document Version:
Publisher's PDF, also known as Version of Record (includes final page, issue and volume numbers)

Please check the document version of this publication:

• A submitted manuscript is the version of the article upon submission and before peer-review. There can be important differences between the submitted version and the official published version of record. People interested in the research are advised to contact the author for the final version of the publication, or visit the DOI to the publisher's website.
• The final author version and the galley proof are versions of the publication after peer review.
• The final published version features the final layout of the paper including the volume, issue and page numbers.

Link to publication

Download date: 05. Oct. 2023

TU/e FUSION
ITER ORGANISATION
INTERNSHIP PROJECT

Microwave detector

Design for ITER

Nick Maassen

Johan W. Oosterbeek

Antoine Sirinelli

Yunxing Ma

Matthew Clough

George Vayakis

Eindhoven, 14 November 2014

Abstract

High power microwaves will be used extensively in ITER for a variety of purposes such as heating, control and diagnostics. Under certain plasma conditions not all power is fully absorbed leading to damage of in-vessel components. A microwave detector based on solid body bolometry has been developed to monitor this non-absorbed power locally in order to protect these components. The detectors can be placed on the vacuum vessel at points of interest such as near sensitive diagnostics or locations where high power densities are expected. This report contains a theoretical as well as a practical description of the proposed detector. A concise overview of all aspects of the design can be found in the summary.

Summary

The two major contributors to the microwave power in the vacuum vessel are the Electron Cyclotron Heating (ECH) and the Collective Thomson Scattering (CTS) with frequencies of 170 GHz and 60 GHz respectively. This power can damage in-vessel components and diagnostics directly through electromagnetic overloading or indirectly through absorption of the power causing overheating. Microwave detectors distributed over the vacuum vessel are proposed to monitor this microwave power and give alerts in case the power density level reaches a critical threshold. The primary goal of these detectors is protection against overheating. The secondary goal is the protection of the sensitive diagnostics, but this is not an absolute requirement. While protection of components and diagnostics has the priority, scientifically there is also an interest in diagnosing the spatial distribution of the microwave power throughout the vacuum vessel. So whenever the primary goal allows it an effort is made to make the detector as sensitive as possible.

The requirement of the detector is to measure power densities as low as 0.5 kW/m^2 up to 1.25 MW/m^2 in steady state and transients up to 3 MW/m^2 for 5.5 s, all with an accuracy of 20 %. This is complicated by the fact that a varying neutron irradiation is present and the constraint that the detectors have to be placed inside spare junction box housings while leaving open the option to replace the detectors by the original junction boxes. The materials that are used also need to be vacuum and neutron irradiation compatible.

The only measurement option that was found to be capable of meeting this requirement is solid body bolometry. Two identical metal bodies, one with a microwave absorbing coating and one bare, are connected in series with a so called differential thermocouple. The voltage over this differential thermocouple is proportional to the temperature difference between the two bodies because of the Seebeck effect. This temperature difference has been related to the microwave power density by the global power balance difference of the bodies and is independent of the neutron irradiation. Cooling of the detector is necessary to allow for a high sensitivity without overheating. Radiative cooling is not possible since it depends on the absolute temperature which is not measured so conductive cooling is applied instead. If the conduction system is symmetric the microwave power density is independent of the surrounding temperature as well.

The solid bodies are be made out of copper for its good thermal conductivity and relatively high melting point. The shape will be cylindrical for ease of manufacturing and to assure a uniform temperature at every height. For this reason the thermocouple wires have to be connected to the cylinder at a single height. The ratio of volume over exposed surface is practically defined by the height of the junction box as 12 mm. This fixes the thermal response time of the copper cylinders at 1.3 s. The response time of the measurement however can be faster at the expense of accuracy if the thermocouples are connected closer to the exposed surface of the cylinders. The requirement of the primary goal however can then no longer be met. The microwave absorbing coating applied on one of the cylinders has the highest known microwave absorption coefficient of 0.81, which is a ceramic composed of alumina and titania also implemented for Wendelstein-7X. This fixes the transient sensitivity at 1.93·10^{-5} Km^2/J or 7.91·10^{-10} Vm^2/J.

The maximum temperature of the cylinders is limited by the sudden decline in the modulus of elasticity of the precipitation hardening iron base super-alloy A286 disc springs at 816 °C. Together with the maximum steady state power this determines the necessary cooling i.e. conduction, which fixes the steady state sensitivity at $5.65 \cdot 10^{-4}$ Km^2/W or $2.32 \cdot 10^{-8}$ Vm^2/W. It is important that the conduction remains constant over the entire temperature range for symmetry in the conduction system. This is achieved by fastening the copper cylinders with a bolt and a disc spring on the junction box base separated by a ceramic washer with a force of 601 N. Two types of bolts have been investigated, namely an alumina M3x7 bolt and a stainless steel M2x8 bolt with a ceramic cover for electrical insulation. With a safety factor of 2, the tensile strength of the alumina bolt is too low to provide the required force. However a copper foil between the ceramic washer and the junction box base should reduce this force to a safe level of 235 N. The conduction of the stainless steel bolt is too strongly temperature dependent to meet the required accuracy and thus only the alumina bolt suffices.

The differential thermocouple type that is chosen is type K, mainly for its linear behavior with an average difference in Seebeck coefficients of 41 μV/°C. This type consists of alumel and chromel wires, both containing at least 90 % nickel. At some point the leads of this differential thermocouple are connected to a copper cable. A temperature difference between these junctions can produce a parasitic signal. This can produce a significant error and is unacceptable. Therefore an isothermal block thermally connecting these junctions is necessary. Both a copper as well as an aluminum nitride block will suffice. For cost effectiveness the copper block is recommended.

Two important aspects of the design have been validated numerically or experimentally. Firstly a microwave detection simulation has been performed using the global power balances of the bodies including most predictable non-linear temperature effects. This simulation confirms that the requirement on the microwave power density can be met with this design. Secondly an experiment involving a differential thermocouple has been performed that validates the concept of connecting two bodies in series with thermocouple wires to measure their temperature difference.

The modifications that have been made to the junction box base are relatively conservative since it also has to house the original junction box. However the junction box lid has been designed freely because it can be replaced. Besides the already planned manufacturing of the junction box housing several new components require custom manufacturing. Both the copper cylinders and the copper isothermal block can be made with standard turning and milling techniques. If the aluminum nitride isothermal blocks are chosen then they have to be custom made by an external company. The ceramic coating can be applied in the same manner as for the bolometers used for Wendelstein-7X, where it is also applied on copper. Finally the disc springs are custom designed and need to be manufactured with precise dimensions from an uncommon spring steel. All other parts are commercially available.

Assembly of the detector should preferably be done in a workshop rather than in the vacuum vessel. This is an important design consideration. Therefore it is important that before installation the spare junction boxes are selected that will be used as microwave detectors so they can be pre-assembled in a workshop. All that remains to be done in-vessel is then the micro-TIG welding of the cable to the differential thermocouple leads, the welding of the junction box base to the vacuum vessel and bolting the lid on the base.

After the assembly of the detectors in the vacuum vessel a collective calibration of all detectors is possible. By sending stray microwave power through the vessel the detectors will start to heat up. When the microwave power is then switched off the detectors will start to cool down and this curve can be analyzed to individually calibrate the conduction of every detector. This way any detector that was broken during installation can also be traced and repaired or removed. Such calibration can be done in a similar way as for the Wendelstein-7X bolometer tested in the MISTRAL by fitting the solution to the global power balance differential equation to the measurement.

Finally an assessment is made whether the goals of the detector have been accomplished. The primary goal was the protection of in-vessel components from overheating. This imposed several requirements on the detector, all of which have been met, and thereby this goal has been achieved. The secondary goal was protection of the sensitive diagnostics. This requires response times in the order of several milliseconds. In the current design the response time is more in the order of a second. This can be improved, but this will be at the cost of accuracy which can then no longer meet the requirements set by the primary goal. Finally an effort was made to use the detector as a diagnostic device for which a minimum microwave power density was defined. This required a very sensitive detector but with a combination of proper cooling and a high maximum temperature this can be achieved. An overview of the specification of the detector is given in *Appendix D*.

Contents

1. Introduction

ITER is an International Thermonuclear Experimental Reactor of the tokamak type. The project aims at building a fusion reactor that produces ten times more energy than is required to sustain the reaction. Inside the tokamak reactor a plasma is heated to temperatures of over a hundred degrees Celsius that are required for the fusion reaction. To form, heat and control this plasma high frequency microwaves are used called Electron Cyclotron Heating (ECH). Sometimes this microwave power is not fully absorbed or not at all in which case it shines through or is reflected towards the tokamak wall. Another microwave bundle is used for a diagnostic system called Collective Thomson Scattering (CTS). This beam is supposed to be unabsorbed by the plasma, only a tiny fraction is scattered for diagnostic reasons. At the wall these microwaves will be reflected throughout the tokamak in the form of a directed beam or as isotropic stray radiation. Either way this power can damage in-vessel components and diagnostics. There are two types of damage that can occur here. The first type of damage is caused directly by the electromagnetic power which can destroy semiconductor devices. The second type causes damage indirectly by absorption of the microwave power which may lead to overheating of components. To protect these components and diagnostics dedicated microwave detectors are designed to monitor the microwaves and give alerts in case the power density level reaches a critical threshold.

In this report several measurement options are investigated and then a microwave detector is designed and analyzed. The primary goal of this detector is protection against overheating of components. The secondary goal is the protection of the sensitive diagnostics, but this is not an absolute requirement. While protection of components and diagnostics has the priority, scientifically there is also an interest in diagnosing the spatial distribution of the microwave power throughout the vacuum vessel. So whenever the primary goal allows it an effort is made to make the detector as sensitive as possible. To translate these goals into a design a list of quantitative requirements is specified.

In the next chapter these requirements are given and a measurement principle is chosen on which the detector is based. After this chapter the theory for this measurement principle is explained and then a basic version of such a detector is analyzed. This detector has been implemented for Wendelstein-7X and has been tested in the MISTRAL facility (MIcrowave STray RAdiation Launch facility). It represents the closest comparison with the proposed ITER microwave detector. In the following chapter the application of this measurement principle to the detector in ITER is discussed. This shows the distinct differences between the detector tested in the MISTRAL and the one used in ITER. In the chapter after that the design and the considerations to come to this design of the detector are discussed. Several options have been left open here that still require some attention. Then an error analysis, a numerical analysis and an experiment are shown that have been performed to validate some unique parts of the design. This is followed by a chapter in which some practical information about the manufacturing, assembly and calibration of the detector is discussed and finally a discussion and a conclusion are presented in the last chapter.

2. Requirements and detector choice

Several measurement options are discussed for their possible application to the microwave detector. To do so they are checked for their compliance with the requirements.

Requirements

ITER will be operated in two different configurations. First there will be an operation in which the plasma is formed in absence of the blankets. In this phase no fusion and thus no neutrons will be produced, but the in-vessel components will be unprotected from the ECH and the CTS. The ECH has a frequency of 170 GHz and the CTS has 60 GHz. Because both sources can damage the in-vessel components both should be measured. During this phase the highest microwave power densities are expected of 1.25 MW/m^2 in steady state and 3 MW/m^2 during startup of 5.5 s[1]. Therefore the microwave detector should have enough cooling and thermal inertia not to exceed the maximum allowable temperature for these cases. The goal of the microwave detector is to be able to measure the maximum expected continuous power density of 1.25 MW/m^2 within 5 s with an accuracy of 20 % in order to give a timely alert so that the ECH or CTS can be switched off in 20 s. This is the time for which the in-vessel components are designed to withstand this power. The second configuration in which ITER will operate is in presence of the blankets. A study of the ratio of microwaves that can penetrate behind the blankets is given in *Appendix A*. For a uniform isotropic stray radiation field the power density in the vessel is 1.7 kW/m$^{2[2]}$ and has a minimum of 0.5 kW/m^2 behind the blankets for a first pass plasma absorption of 99 %. This power density might overheat some components over time with poor cooling. Therefore this minimum should also be measured but now it may be done within a time limit as long as 60 s with an accuracy of 20 %. Furthermore in this last phase neutron radiation will be present up to 3·10^{14} n/m^{2}s with energies of 14 MeV and 2·10^{16} n/m^{2}s with energies larger than 0.1 MeV[3]. These neutrons will heat the in-vessel components together with the microwaves but other detectors are dedicated to measure the neutron radiation and the microwave detector should not be affected by the neutron heating. Also neutron radiation will alter some material properties yet these specifications should still be met. Furthermore a changing magnetic field in the radial direction of 0.1 T/s[4] should be expected. Finally the vacuum vessel design has already been "frozen" so that no new diagnostics can be placed inside the vessel. This means that the detector has to be placed inside the spare junction boxes while leaving open the option to remove the detector and use them as a junction box. Images of the original junction box are given in *Appendix B*. A summary of the requirements is given in *Table 1*.

Table 1: Summary of the requirements for the microwave detector.

Requirement	Value
Survive maximum startup microwave power	3 MW/m^2 for 5.5 s
Survive maximum steady state microwave power	1.25 MW/m^2
Measure maximum microwave power	1.25 MW/m^2 within 5 s with an accuracy of 20 %
Measure minimum microwave power	0.5 kW/m^2 within 60 s with an accuracy of 20 %
Compensate for maximum neutron irradiation	3·10^{14} n/m^{2}s with energies of 14 MeV and 2·10^{16} n/m^{2}s with energies larger than 0.1 MeV
Compensate for changing radial magnetic field	0.1 T/s

Measurement options

The most common detector used for measuring microwave power is a standard microwave engineering Schottky-diode detector[5]. This diode alone however discriminates between different polarizations and is sensitive to field patterns of the order of wavelengths. To solve these limitations the diode is embedded in a so-called sniffer probe. A sketch of such a sniffer probe is shown in *Figure 1*. It basically is a waveguide that picks up microwave power and leads it into a metal sphere[6]. In this sphere, the radiation reflects and a microwave power field builds up. The diode is then placed on this sphere where it can measure the microwave power. The idea is that the spherical resonator causes averaging over all angles and polarizations so that the measured signal only depends on the power of the incoming microwaves. This method has the advantage of having a very fast response time due to the direct conversion of microwave power into a voltage in the diode. The disadvantage is that diodes are semiconductors which need to be shielded very well from neutrons. Moreover, in practice it has so far not been possible to obtain sufficient scrambling to accurately measure the microwave power. Improved scrambling can be obtained by scaling the waveguide and the sphere to very large dimensions in the order of meters[5], but this would require significant changes to the diagnostic layout.

Sferical Copper cavity (D > 140 λ)

Solid state Detector

Quartz vacuum window

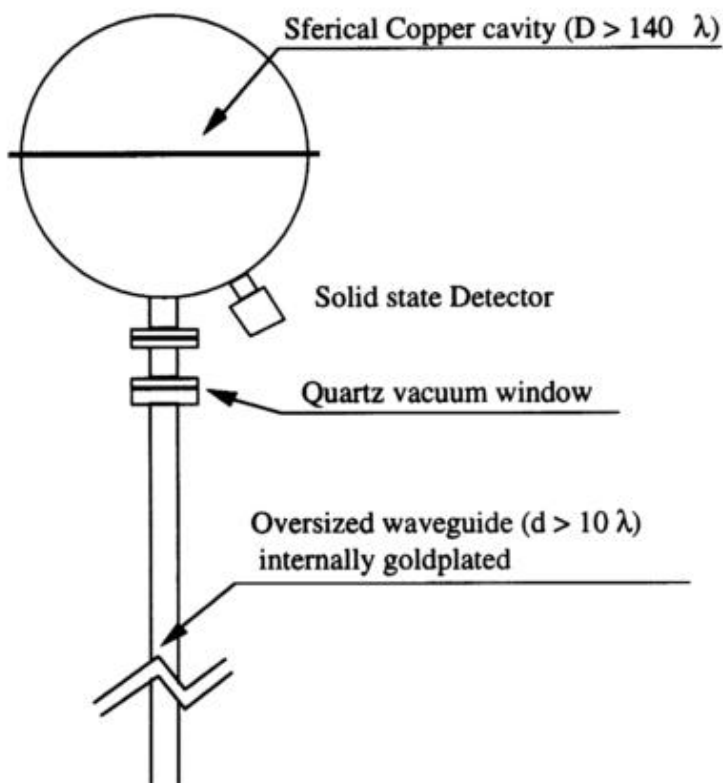Oversized waveguide (d > 10 λ) internally goldplated

Figure 1: Sketch of the sniffer probe components. It consists of a metal waveguide, a metal sphere and a Schottky-diode detector[5].

Another possibility is to use far infrared pyroelectric sensors[5]. A sketch of a pyroelectric sensor is shown in *Figure 2*. A pyroelectric sensor relies on the indirect pyroelectric effect of certain crystalline substances to transform heat flow into electric charge. A differential voltage can then be recorded as a function of the power flux. The built-up charge decays exponentially over time due to the finite internal resistance of the crystal. The output therefore cannot be used directly to determine the incident power flux but it must be integrated. The response time of this sensor is very fast around ten milliseconds[5]. The downside is that this sensor experiences drifts due to the integration that is necessary. Also the applicability of these sensors as microwave detectors has not been investigated in detail yet. For ITER however this method will probably be difficult due to neutron irradiation which can damage the pyroelectric crystal and the electrical circuit and can cause unresolvable heat disturbances in the crystal.
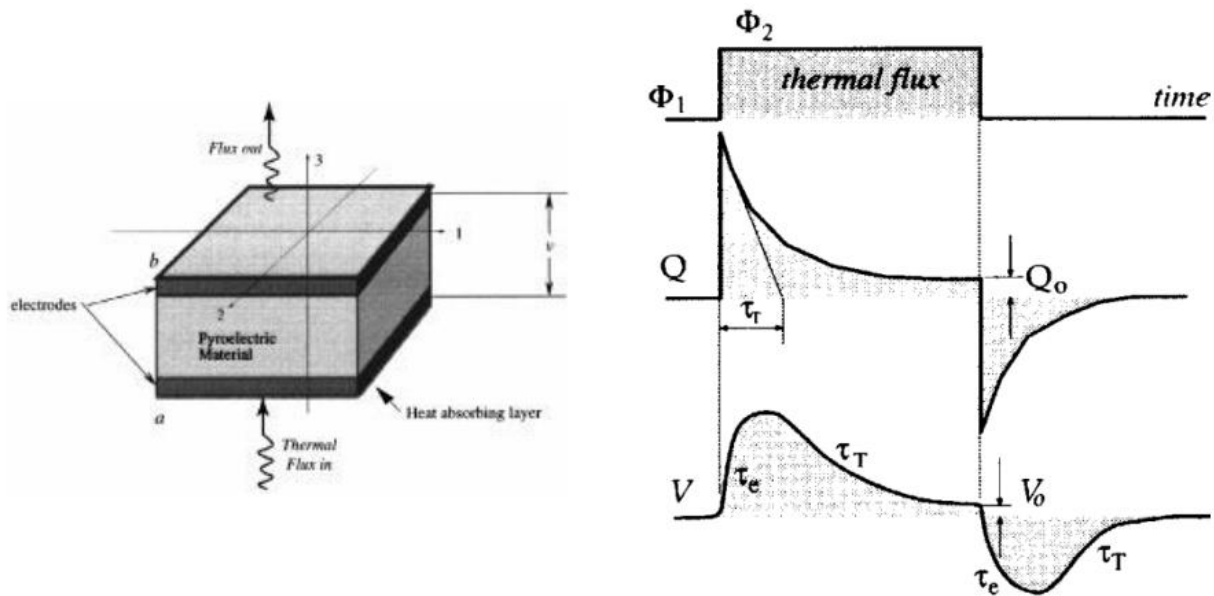
Figure 2: Sketch of the measurement principle of a pyroelectric thermometer[5]. The measured signal has to be integrated to determine the incoming microwave power.

Finally there is the option of bolometry. A sketch of the bolometer principle is given in *Figure 3*. The working principle is that the microwave power is absorbed by a fluid or a solid whose temperature rise can be measured with an RTD (Resistance Temperature Detector) or a thermocouple[5]. The voltage should then be differentiated to find the microwave power. This very simple and robust principle also has the advantage of a very stable output and an absolute calibration. The disadvantage is the slow response time which can be as long as a second for reliable measurements and it will be difficult to protect sensitive diagnostics with this method.
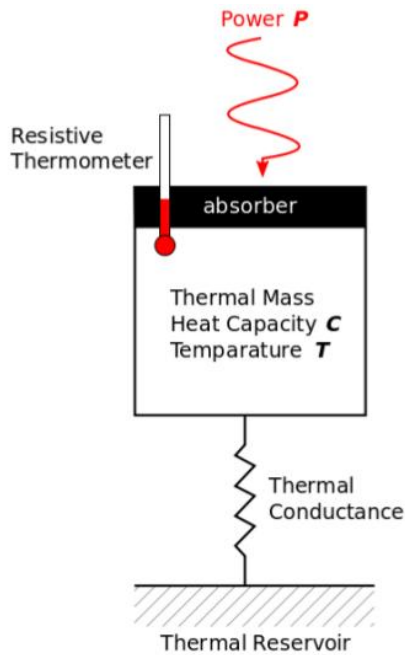
Figure 3: Sketch of the measurement principle of a bolometer[5]. Conduction is used here for cooling.

There is an important difference between a fluid and a solid bolometer. A fluid bolometer absorbs the microwave power volumetrically and can have absorptions coefficients up to a 100 % for deep enough volumes[7]. This does not require an absorption coefficient to be determined and makes the measurement frequency independent. There are however two problems with this method. First the temperature deposition is not uniform (exponentially actually) which causes temperature gradients that drive convective transport. This makes measuring the average temperature very difficult so a stirring device is required. This in turn makes the device more complex and too large to fit in a junction box. Secondly neutron irradiation will also cause volumetric heating which makes it indistinguishable from the microwave radiation. An example of a fluid bolometer is shown in *Figure 4*.
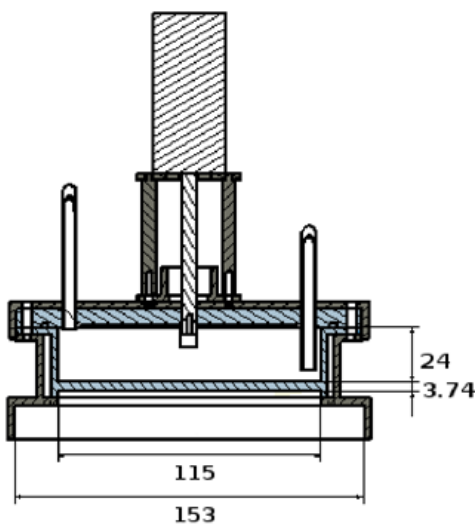
Figure 4: Cross-section of a fluid bolometer. The dimensions are in millimeters[7].

Both these problems can be solved with solid body bolometry. In a solid body bolometer the microwaves are partly absorbed and partly reflected at the surface. This makes the power deposition even less uniform but if a well conducting solid is used then the temperature gradients will be minimal and a reliable temperature reading can be made from anywhere on the solid body. Secondly because the microwave absorption is only in the surface a distinction between neutron and microwave radiation can be made. This is done by having two identical solid bodies, one coated with a microwave absorbing coating and one with a reflecting coating (or bare)[8]. The neutron irradiation will heat both bodies equally while the microwaves heat one more than the other. The difference in temperature rises of the two bodies is then a measure for the microwave power only. This can be measured with a differential thermocouple. Even though the response time may be too long for protection of sensitive diagnostics it does qualify for all other requirements. This is the basic principle on which the design of the microwave detector is based. The basic concept of such a bolometer is shown in *Figure 5*.

Figure 5: Concept of a stray radiation monitor based on a bolometer[8]. The difference in temperature between the two bodies is a measure for the microwave power and is measured with a differential thermocouple.

3. Theory

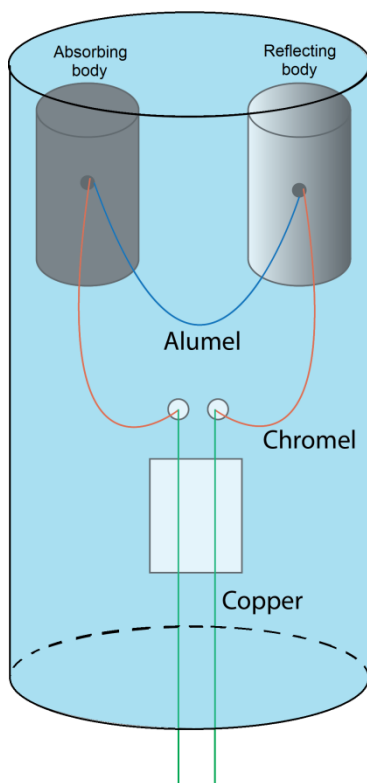The goal of the microwave detector is to measure the microwave power density p. This has to be deduced from the output of the detector, which is a voltage ΔV. For a detector based on bolometry there is an intermediate quantity which is the temperature T. A relation between the temperature T and the voltage ΔV can be found with the thermo-electric Seebeck effect. The general theory for this effect is discussed first. After this the relation between the microwave power density p and the temperature T is discussed. This is described by the power balance which is explained here generally.

Seebeck effect

First Ohm's law and the Seebeck effect are combined and are then rewritten to find a practical integral equation. The general form of Ohm's law gives a proportional relation between the current density $\vec{J}$ and the electric field $\vec{E}$

$$\vec{J} = \sigma\vec{E}, \tag{3.1}$$

where σ is the electrical conductivity of the medium. An electric field $\vec{E}$ can be produced by two mechanisms. The first is by applying an external voltage to the medium which causes a gradient in the potential $\vec{\nabla}V$ and the second is by means of an electromotive force $\vec{\mathcal{E}}$, that is produced without external intervention

$$\vec{E} = \vec{\mathcal{E}} - \vec{\nabla}V. \tag{3.2}$$

One way to produce such an electromotive force $\vec{\mathcal{E}}$ is the Seebeck effect. This converts a temperature gradient $\vec{\nabla}T$ directly into an electromotive force $\vec{\mathcal{E}}$[9]

$$\vec{\mathcal{E}} = -S\vec{\nabla}T, \tag{3.3}$$

with the proportionality constant S called the Seebeck coefficient. Substituting equations (3.2) and (3.3) into equation (3.1) yields

$$\vec{J} = \sigma\left(-S\vec{\nabla}T - \vec{\nabla}V\right). \tag{3.4}$$
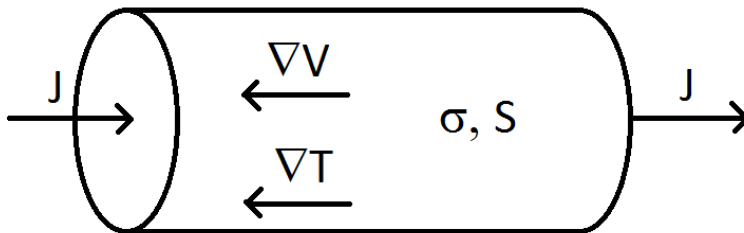
This equation in visualized in *Figure 6*.

Figure 6: Illustration of the Seebeck effect in a piece of wire. The material properties are the electrical conductivity σ and the Seebeck coefficient S. A gradient in the potential $\vec{\nabla}V$ or in the temperature $\vec{\nabla}T$ produces a current density $\vec{J}$.

To use the Seebeck effect to find the temperature by measuring a voltage the first step is to eliminate the possibility of a current $\vec{J} = 0$. This is possible if the electrical circuit is an open loop or if the resistance of the voltage measurement is very high. The result is the following equation

$$-\vec{\nabla}V = S\vec{\nabla}T. \tag{3.5}$$

In the one dimensional case where only one electrical path is possible the equation reduces to

$$-\frac{dV}{dx} = S\frac{dT}{dx}. \tag{3.6}$$

where x is the coordinate following the electric path. Integrating over this electrical path results in an expression for the voltage as a function of temperature

$$\Delta V = -\int dV = \int S dT. \tag{3.7}$$

The minus sign has been introduced to simplify the equation and this will mean in practice that the electrodes of the voltmeter are swapped to read a positive voltage.

Power balance

Now all that remains is to link the temperature T to the microwave power density p. This is done with the power balance. In order to simplify the power balance as far as possible the body should have a uniform temperature at every instant of time. This means that the lumped capacitance method can be used which ignores spatial effects. In order to validate the use of this lumped capacitance method first the Biot number should be calculated. This is the ratio of the internal thermal resistance of the body to the thermal resistance of the boundary layer. In the absence of convection (true in case of a vacuum) only conduction and radiation can transfer heat. Two types of radiation are considered here, microwave radiation and heat exchange due to surfaces with different temperatures. The Biot number Bi is defined as[10]

$$Bi = hL_c/k_{int}, \tag{3.8}$$

where L_c is the ratio between the volume of the body V and the surface that is exposed S ($L_c = V/S$) and k_{int} is the internal thermal conductivity. Finally h is the heat transfer coefficient, which is defined as

$$h = \frac{q}{T - T_{sur}}, \tag{3.9}$$

according to Newton's law of cooling. Here q is the total heat flux, T is the temperature of the considered object and T_{sur} is the temperature of the surrounding. The maximum total heat flux q in the body is

$$q = q_\mu - q_r + q_c, \tag{3.10}$$

where q_μ, q_r and q_c are the heat fluxes of the microwaves, the radiation and the conduction respectively.

An image of these heat fluxes is shown in *Figure 7*.
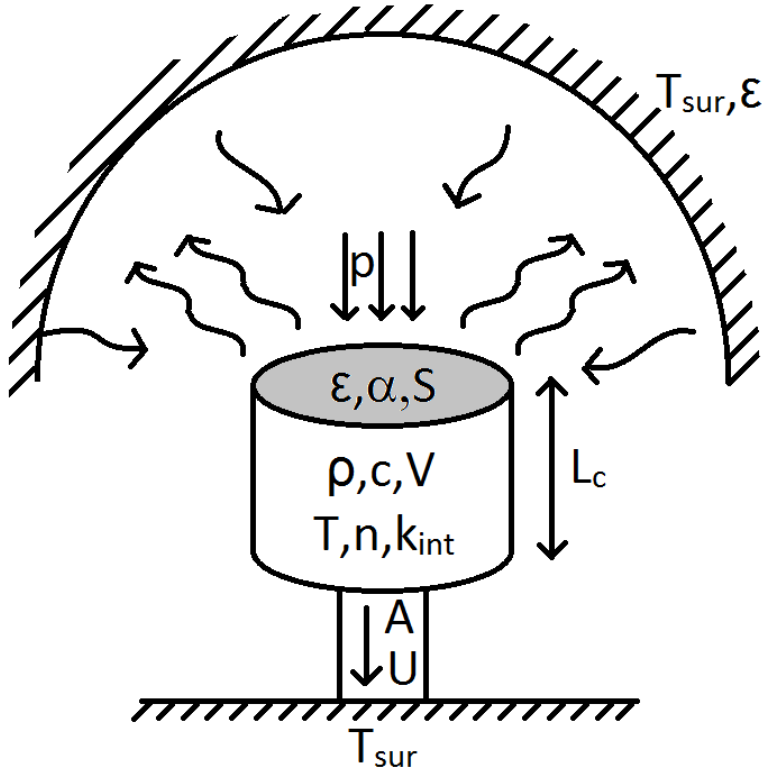
Figure 7: Illustration of the power balance in a solid body. The volumetric material properties are the density ρ, the specific heat capacitance c and the internal thermal conductivity k_{int}. The exposed surface has an emissivity ε and a microwave absorption coefficient α. The geometric properties of the body are the volume V, the exposed surface S and the ratio between these L_c. Heating of the body is by microwave power p and neutronic heating n. The surroundings of the body have a temperature T_{sur}, an emissivity ε and conducting area A. The loss of heat to the surroundings is by heat radiation $\varepsilon\sigma$ and conduction U.

The microwave power p can be related to an incoming heat flux q_μ with the absorption coefficient α of the surface of the body

$$q_\mu = \alpha p. \tag{3.11}$$

The net heat transfer by thermal radiation q_r from the body can be approximated as[10]

$$q_r = \varepsilon\sigma(T^4 - T_{sur}^4), \tag{3.12}$$

where ε is the emissivity of the surface of the body and σ is the Stefan-Boltzmann constant ($\sigma = 5.67 \times 10^{-8} W/m^2K^4$). And finally the conduction heat flux q_c can be quantified as

$$q_c = U(T - T_{sur})/A, \tag{3.13}$$

where U is the overall heat transfer coefficient through conduction and A is the area through which the heat is conducted.

Substitution of equations (3.9-3.13) into equation (3.8) gives the expression for the Biot number

$$Bi = \frac{L_c}{k_{int}} \left| \frac{\alpha p}{T - T_{sur}} - \varepsilon\sigma(T + T_{sur})(T^2 + T_{sur}^2) + \frac{U}{A} \right|. \tag{3.14}$$

As a rule of thumb the Biot number should be smaller than $Bi < 0.1$ to avoid large errors in using the lumped capacitance method (0D power balance)[10].

Another important dimensionless number that should be kept in mind is the Fourier number. This is the ratio of the heat conduction rate to the rate of thermal energy storage in a solid and it represents a dimensionless time. It is defined as[10]

$$Fo = \frac{k_{int}\tau}{\rho c L_c^2}, \tag{3.15}$$

where τ is the response time, ρ is the density and c is the specific heat capacity. For a characteristic response time τ the Fourier number is $Fo = 1$[10]

$$\tau = Fo\frac{\rho c L_c^2}{k_{int}} = \frac{\rho c L_c^2}{k_{int}}. \tag{3.16}$$

Now the power balance of the solid body can be formed. The lumped capacitance method allows the analysis to be done zero dimensional. The terms that increase the temperature T are the neutron irradiation power P_n and the total microwave power $q_\mu S$. The terms that transfer this heat away are heat radiation $q_r S$ and conduction $q_c A$. The change in temperature is then written as[10]

$$\rho c V\frac{dT}{dt} = P_n + (q_\mu - q_r)S - q_c A. \tag{3.17}$$

The neutron power absorption is considered minimal and the neutron power density is therefore constant in space. Neutrons are not reflected like microwave but are transmitted which means that the neutrons act as a volumetric heating source

$$P_n = nV, \tag{3.18}$$

where n is the neutron power density per unit of volume. Putting equations (3.11-3.13) and equation (3.18) together into equation (3.17) yields the total power balance

$$\rho c V\frac{dT}{dt} = \alpha p S + nV - \varepsilon\sigma S(T^4 - T_{sur}^4) - U(T - T_{sur}). \tag{3.19}$$

4. Wendelstein-7X detector analysis

A solid body bolometer designed for Wendelstein-7X[11] is now analyzed. This detector has been tested in the MISTRAL facility and represents the closest comparison with the proposed ITER microwave detector. The theory is applied here to find out how well it is suited to translate actual measurements to the microwave power density. The main difference between this detector and the ITER detector is that neutron radiation is absent and only a single graphite body is used. Conduction will also be minimal and only possible through a thin thermocouple. An image of this detector is shown in *Figure 8*.

Figure 8: Picture of the graphite bolometer used in the MISTRAL to measure the microwave power[12]. The height and the diameter are both 10 mm.

First the thermo-electrical system is explained (a standard thermocouple) and then an estimate is made of all terms in the power balance. Then the power balance is applied to determine the microwave power density both post experimentally as well as real time.

Thermocouple analysis

In the MISTRAL a standard thermocouple is used to determine the temperature of the body. The working principle of a thermocouple is based on the Seebeck effect. How this is used to determine the absolute temperature of the body is explained here.

The Seebeck effect can only be used to measure temperature differences. So to determine an absolute temperature T_m, at one point the temperature must be known. This is the reference temperature T_{ref}. Leading a wire between these two points creates the voltage

$$\Delta V = \int_{T_{ref}}^{T_m} S dT.$$

(4.1)

However to measure this voltage it is inevitable that a wire has to be led back to the reference temperature T_{ref} creating an electromotive force E_{emf} that exactly opposes the electromotive force that is desired.

$$\Delta V = \int_{T_{ref}}^{T_m} S dT + \int_{T_m}^{T_{ref}} S dT = 0.$$

(4.2)

And thus nothing is measured. This could be solved by using a superconducting wire which cannot sustain a voltage over its length[13], but this is not practical. It is better to use two wires of type A and B that have different Seebeck coefficients S_A and S_B as is shown in *Figure 9*.
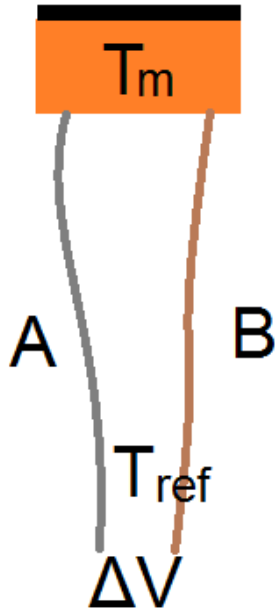
Figure 9: Schematic representation of a thermocouple connected to a solid body. The thermocouple consists of two wires A and B with different Seebeck coefficients. This temperature T_m can be determined by measuring the voltage ΔV at temperature T_{ref}.

For this configuration the measured voltage is

$$\Delta V = \int_{T_{ref}}^{T_m} S_A dT + \int_{T_m}^{T_{ref}} S_B dT = \int_{T_{ref}}^{T_m} (S_A - S_B)\, dT. \tag{4.3}$$

So for known Seebeck coefficients S_A and S_B as function of temperature T, a known reference temperature T_{ref} and a measured voltage ΔV, the temperature T_m can be determined. This is the working principle of a standard thermocouple.

Power balance analysis

In order to find out if any terms in the power balance can be neglected and whether the lumped capacitance method is valid an estimate is made of all terms and the Biot number is calculated. The Biot number cannot be calculated beforehand since the power density of the microwaves is unknown but it will be calculated afterwards to validate the results. The thermocouple is modeled as a one dimensional wire with area A and length L. The overall heat transfer coefficient U of the thermocouple is then

$$U = \frac{kA}{L}. \tag{4.4}$$

The values for the required variables that are used to make the estimates are shown in *Table 2*.

Table 2: Parameters obtained from the graphite body tested in the MISTRAL [12].

Variable	Symbol	Value
Volume of body	V	0.79 cm^3
Surface of body	S	4.71 cm^2
Thermal conductivity of body	k_{int}	80 W/mK
Thermal conductivity of wire	k	40 W/mK
Surrounding temperature of vessel	T_{sur}	292 K
Microwave absorption coefficient of body	α	0.07
Emissivity of body	ε	0.81
Stefan-Boltzmann constant	σ	5.67x10^{-8} W/m^{2}K^4
Density of body	ρ	1805 kg/m^3
Specific heat capacity of body	c	715 J/kgK
Area of wire	A	0.79 mm^2
Length of wire	L	2 m
Neutron power density	n	0 W/cm^3

With this data also the characteristic response time can be calculated and is $\tau = 0.07$ s. This is approximately the delay of the measurement system and this is shorter than the sampling time of 90 ms, but not by much so a single sample should not be seen as an accurate measure of the temperature.

First the power balance is considered during cool down, so in absence of microwave power $p = 0$. During this interval the Biot number can be calculated and at the maximum of $T = 386$ K it is $Bi = 1.9 \cdot 10^{-4}$. This is very low and the lumped capacitance method can be used with a negligible error.

Now an experiment on the detector is analyzed[14]. In this experiment isotropic microwave radiation with a constant power is applied in certain intervals for certain periods. *Figure 10* shows the time interval in which the estimation of the power density is done.
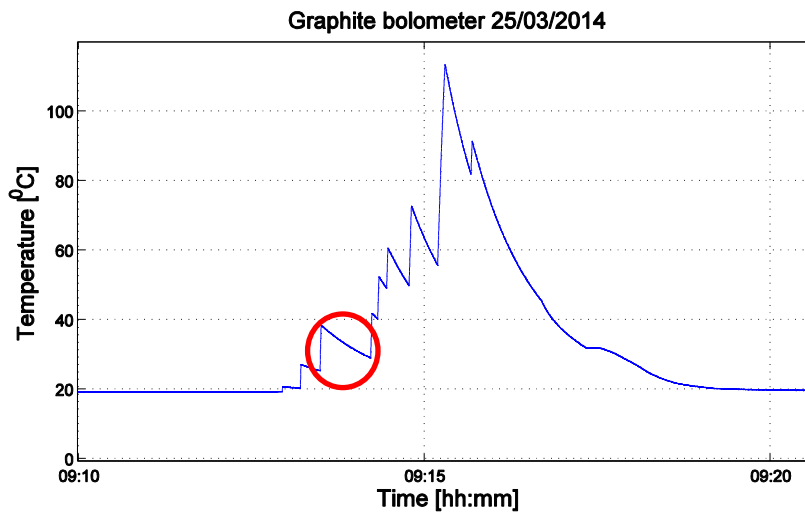

Figure 10: In blue the plot of temperature against time for the graphite body tested in MISTRAL. In red is the area for which the microwave power density is calculated.

During the cool down phase the temperature drops from $T = 312$ K to $T = 302$ K in $t = 408$ s. The internal power loss is then approximately 25 mW. The losses are estimated using the average temperature $T = 307$ K. This results in a radiation loss of approximately 74 mW, which is obviously impossible since the temperature does not drop that much but this is only an estimate. The conduction loss through the wire is estimated at only 0.2 mW. This means that even at relatively low temperatures radiation dominates the loss term and conduction losses are negligible. The change in temperature is therefore entirely attributed to the radiation losses. Now the heating phase is analyzed. The temperature rises from $T = 298$ K to $T = 311$ K in exactly $t = 10$ s. The internal power gain is then calculated as 1341 mW. In this phase the radiation loss (which is approximately the same as during the cool down phase) is negligible. The power density of the microwaves is now approximately $p = 40.7$ kW/m^2. The maximum Biot number can now also be calculated and is $Bi = 5.9 \cdot 10^{-4}$ which is still low enough to use the lumped capacitance method.

Post-experimental determination of power density

Once the experiment is over the whole data range can be analyzed and used to determine the power density p. This allows the determination to be as precise as possible. To do so a general solution to the power balance is fitted to the acquired data. The fact that the (global) power balance equation is an ordinary differential equation that can be solved analytically makes this easier. First it is rewritten

$$\rho c V \frac{dT}{dt} = \alpha p S - \varepsilon \sigma S (T^4 - T_{sur}^4), \tag{4.5}$$

$$\frac{dT}{dt} = \frac{\varepsilon \sigma S}{\rho c V} \left(\frac{\alpha p}{\varepsilon \sigma} + T_{sur}^4 - T^4 \right) = \frac{\varepsilon \sigma S}{\rho c V} \left(T_{eq}^4 - T^4 \right) \quad \wedge \quad T_{eq}^4 = T_{sur}^4 + \frac{\alpha p}{\varepsilon \sigma}, \tag{4.6}$$

where T_{eq} is the equivalent surrounding temperature if all incoming power came only from radiation of the surrounding. Next this equation can be solved by separation of variables and integration

$$\int \frac{dT}{T_{eq}^4 - T^4} = \frac{\varepsilon \sigma S}{\rho c V} \int dt, \tag{4.7}$$

$$\frac{\arctan{(T/T_{eq})} + \operatorname{arctanh}{(T/T_{eq})}}{2 T_{eq}^3} = \frac{\varepsilon \sigma S}{\rho c V} (t + t_0). \tag{4.8}$$

In absence of microwave heating $p = 0$ during the cooling down phase and $T_{eq} = T_{sur}$ and is known. The constant $\varepsilon \sigma S / \rho c V$ can now be determined by using the following transformation

$$y = \frac{\arctan{(T/T_{eq})} + \operatorname{arctanh}{(T/T_{eq})}}{2 T_{eq}^3} = \frac{\varepsilon \sigma S}{\rho c V} (t + t_0), \tag{4.9}$$

in which y depends linearly on t. The slope can now determine the constant

$$\frac{dy}{dt} = \frac{\Delta y}{\Delta t} = \frac{\varepsilon \sigma S}{\rho c V}. \tag{4.10}$$
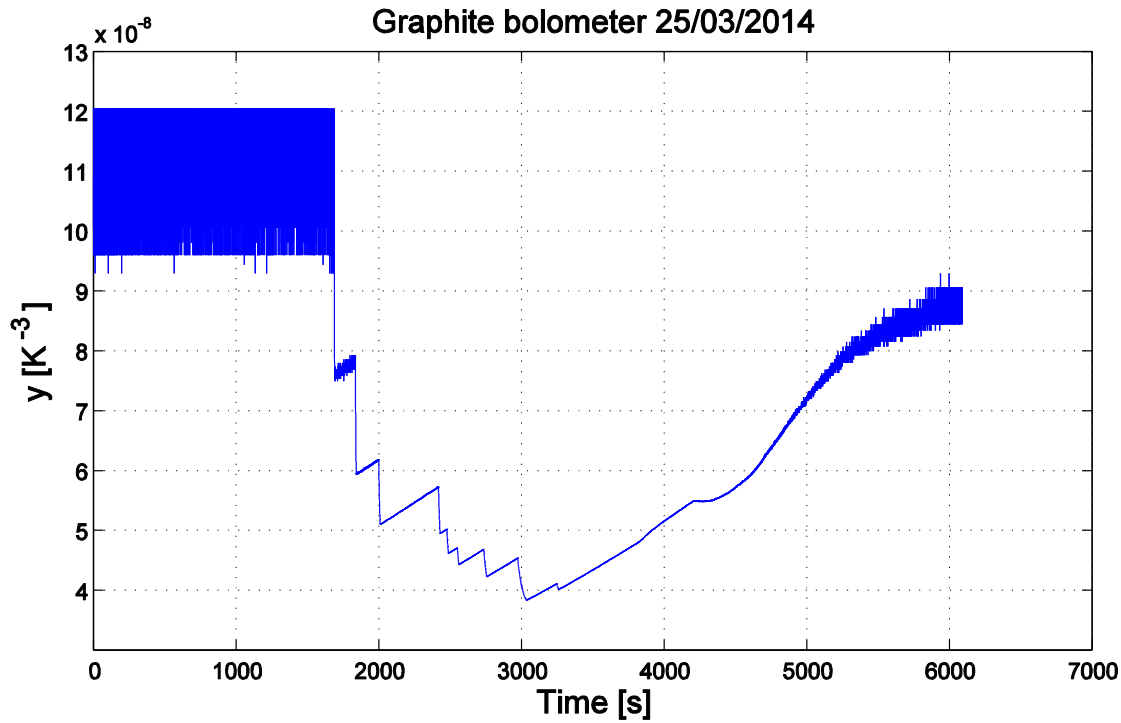
The transformation is shown in *Figure 11*.

Figure 11: The transformation of the y-axis for calibration of the radiation heat loss.

During the cool down phase y should increase linearly. This is visible in the figure. A fit can be made through the linear part to determine the constant. This has been done and results in $\varepsilon\sigma S/\rho cV = 1.55 \cdot 10^{-11}$ K^{-3}s^{-1}.

Now the same equation can be used for the microwave heating phase. But now the equivalent temperature T_{eq} is not known beforehand and it is required to find the microwave power density p. There is no explicit formulation for T_{eq} so this has to be solved numerically. This can be done in the same manner as before in the estimation by determining the temperature before and after heating. The values used remain the same. This results in an equivalent temperature $T_{eq} = 551$ K. This means that if the surrounding vacuum vessel would be heated to this temperature no microwave power would have to be supplied to simulate the temperature profile. The microwave power density p can be found by

$$\frac{\alpha p S}{\rho cV} = \frac{\varepsilon\sigma S}{\rho cV}\left(T_{eq}^4 - T_{sur}^4\right). \qquad (4.11)$$

This value is then $\alpha p S/\rho cV = 1.31$ K/s. The microwave power density can then be determined as $p = 41.46$ kW/m^2. The power density without including the radiation loss is $p = 40.96$ kW/m^2 so in this case there is a 1.5% error in neglecting this. This seems to be a reasonable assumption in order to avoid the complexity of solving a nonlinear equation but as the temperature gets higher the radiation losses go with the power of four and this quickly becomes more important.

This is shown in the reconstruction of the temperature profile shown in *Figure 12*.
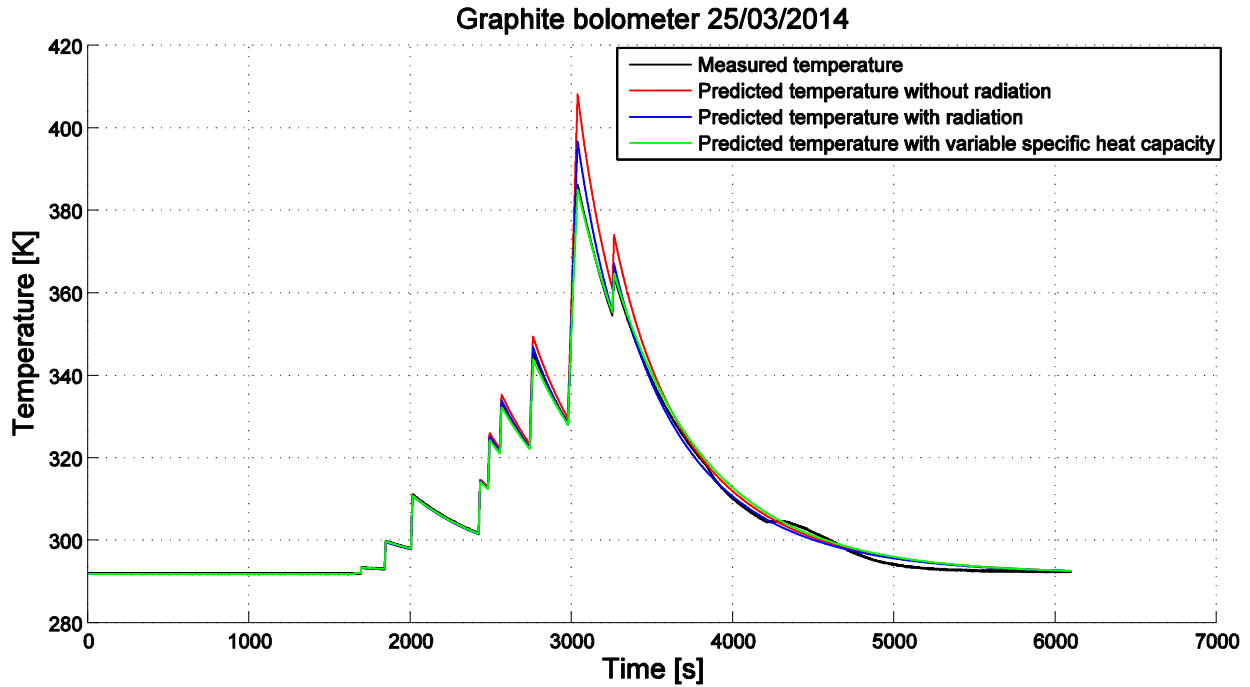

Figure 12: Plot of temperature against time for the graphite body tested in MISTRAL. The black line is the measured temperature, the red line is the predicted temperature neglecting radiation losses during heating, the blue line does include these losses and the green line also incorporates a variable specific heat capacity.

As is visible at low temperatures neglecting the radiation losses during heating causes little deviation from the measurements, but at higher temperatures the difference does become significant. Even so there still is a difference between the measured temperature and the predicted temperature at higher temperatures. This is caused by the fact that the specific heat capacity c in reality is not constant but scales approximately linear with temperature below 500 K[10]. With a variable heat capacity the predicted temperature almost perfectly matches the measured temperature. The strange behavior that starts at about 4000 s is caused by the ventilation of the vacuum vessel and some other irrelevant tests.

Real-time determination of power density

While a post-experimental analysis of the data allows the most accurate determination of the power density this is not possible when a real-time measurement is required. This method also assumes that the microwave power density is constant, which may be correct for this experiment but for an actual microwave detector this cannot be assumed. Therefore the power balance is applied directly instead of solving it to find the microwave power density as a function of time

$$\frac{\alpha p S}{\rho c V} = \frac{dT}{dt} + \frac{\varepsilon \sigma S}{\rho c V}(T^4 - T_{sur}^4). \tag{4.12}$$

This equation requires the numerical calculation of a derivative. This is very sensitive to the noise on the temperature measurement so this is smoothed out first by integration over time. The integration should be kept to a minimum to avoid loss of data but should also be enough to reduce the noise on the results. The results are shown in *Figure 13*.
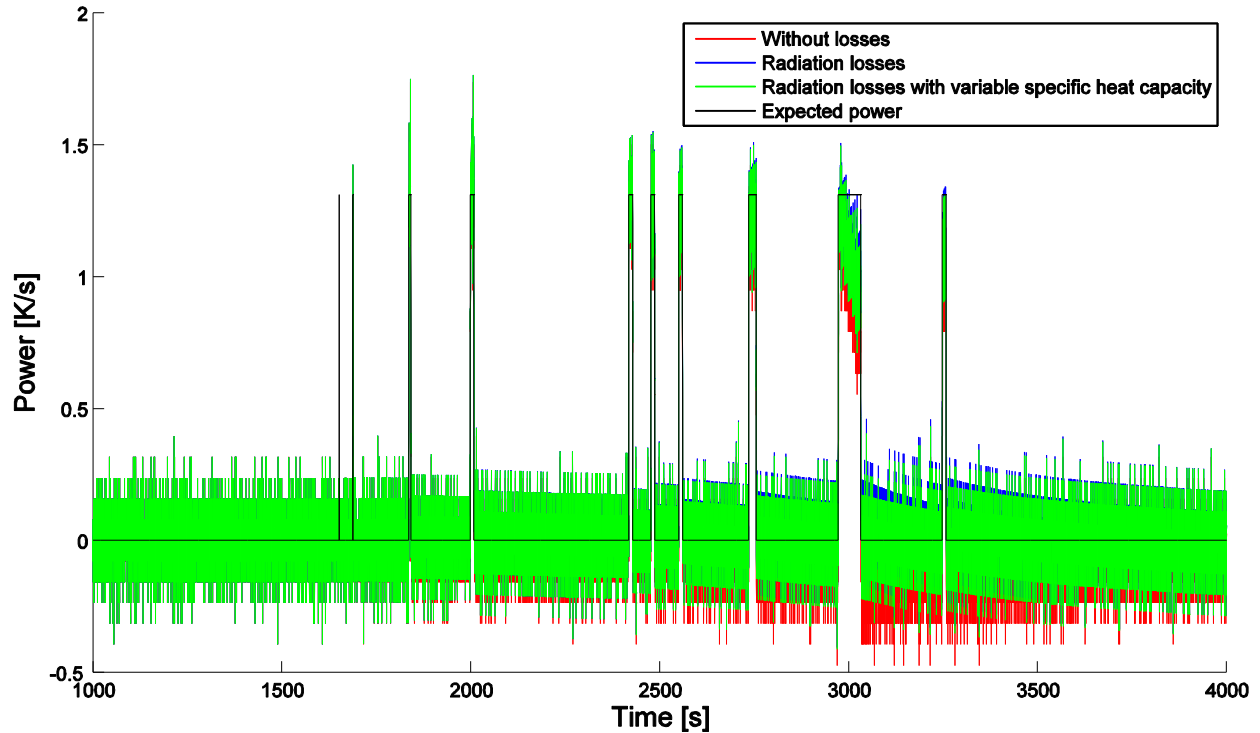
Figure 13: Plot of microwave power against time for the graphite body tested in MISTRAL. The red line is the predicted power neglecting radiation losses, the blue line does include radiation losses, the green line also incorporates a variable specific heat capacity and the black line is the predicted microwave power.

In red is the calculated microwave power density without including the radiation losses. This means that the entire change in temperature is contributed to the microwaves, so when the temperature decreases the microwave power density has to be negative. In blue is the microwave power density corrected for radiation and in green is the corrected power density with a variable specific heat capacity. In black the microwave power as calculated before is shown. The best results are from the longer heating pulses because the smoothing is less influencing the derivative and at low temperatures because the specific heat capacity is constant. This evaluation can be done real time so it is more suitable for control purposes and for variable microwave power densities. This way the power density can be determined as $\alpha p S / \rho c V = 1.14 \pm 0.20$ K/s or $p = 35 \pm 6$ kW/m^2. Compared to $p = 41.46$ kW/m^2 as previously determined this is just within one standard deviation.

5. ITER detector

The theory applied for the detector designed for Wendelstein-7X can be applied in a similar way to the ITER detector but with the complications caused by the two solid bodies. The two bodies are necessary to measure the microwave power independent from the neutron irradiation[8]. First the differential thermocouple is explained that is used to measure the difference in temperatures between the two bodies. Then the power balances of both bodies are rewritten to find a relation between the difference in temperatures and the microwave power density.

Differential thermocouple concept

In the ITER detector the interest is not in absolute temperatures but in a temperature difference between two bodies. Of course it is possible to just measure both temperatures independently with standard thermocouples, but this requires twice the cabling and thus twice the interference that can cause an error. Therefore a different measurement system is used called a differential thermocouple.

A differential thermocouple measures the temperature difference directly. To do so a wire of type B connects the voltmeter to body 1, a wire of type A connects body 1 and 2 and another piece of type B connects body 2 to the voltmeter again. This configuration is shown in *Figure 14*.
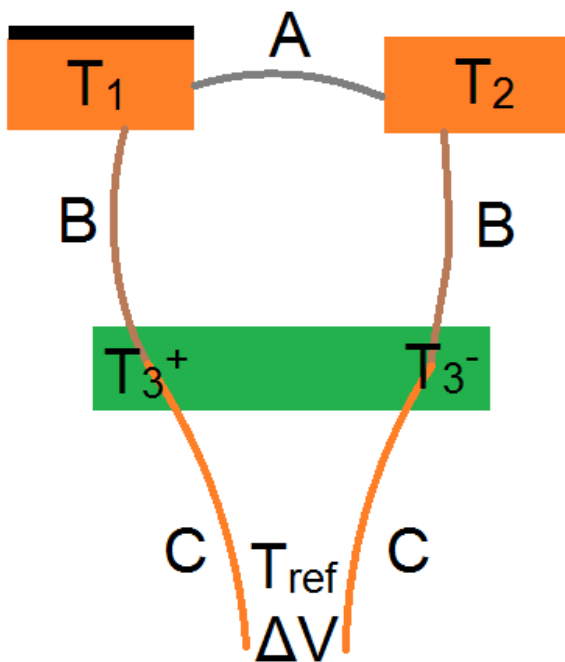
Figure 14: Schematic representation of a differential thermocouple connecting two solid bodies. This differential thermocouple consists of two wire types A and B. They are connected in series with the two bodies to determine the temperature difference $T_1 - T_2$ by measuring the voltage ΔV independent from the reference temperature T_{ref}. Connecting the leads of the thermocouple to wire type C causes a parasitic voltage at the junctions with temperatures T_3^- and T_3^+.

This gives the following voltage ΔV

$$\Delta V = \int_{T_{ref}}^{T_1} S_B dT + \int_{T_1}^{T_2} S_A dT + \int_{T_2}^{T_{ref}} S_B dT = \int_{T_1}^{T_2} (S_A - S_B) dT. \tag{5.1}$$

Now however the temperature difference $T_2 - T_1$ cannot be determined from the voltage ΔV because the Seebeck coefficients depend on the absolute temperature T which is not measured. The solution to this is to make sure that the difference in Seebeck coefficients $S_A - S_B$ is constant in the temperature range from T_1 to T_2, in which case the voltage no longer depends on the absolute temperature

$$\Delta V = (S_A - S_B)(T_2 - T_1). \tag{5.2}$$

The materials for which the difference in Seebeck coefficients is constant in temperature however may not be ideal for leading a cable all the way back to the voltmeter, so preferably another wire type C is used for this. The temperatures T_3^- and T_3^+ in the junctions between types B and C however now also start to function as thermocouples, causing a parasitic signal

$$\Delta V = \int_{T_{ref}}^{T_3^+} S_C dT + \int_{T_3^+}^{T_1} S_B dT + \int_{T_1}^{T_2} S_A dT + \int_{T_2}^{T_3^-} S_B dT + \int_{T_3^-}^{T_{ref}} S_C dT, \tag{5.3}$$

$$\Delta V = \int_{T_1}^{T_2} (S_A - S_B) dT + \int_{T_3^-}^{T_3^+} (S_C - S_B) dT, \tag{5.4}$$

$$\Delta V = (S_A - S_B)(T_2 - T_1) + (S_C - S_B)(T_3^+ - T_3^-). \tag{5.5}$$

The difference in Seebeck coefficients $S_C - S_B$ in the parasitic signal should be evaluated at the temperature average of the junctions T_3. The parasitic effect can be reduced by making sure that the junctions are isothermal $T_3^- = T_3^+$. Also by choosing the difference in Seebeck coefficients between types A and B to be as large and the difference between types B and C as small as possible will reduce the effect.

Power balance difference

In ITER there will be long pulses of up to a thousand seconds. The microwave detector should be able to detect microwaves accurately over the whole period which means that a significant temperature rise is required. This in turn causes the danger of overheating so cooling is necessary. In presence of a vacuum there are two methods of cooling, namely conduction and radiation. Radiation is favorable because it starts to cool more at higher temperatures with the power of four but this non-linearity causes problems in determining the amount of radiation through only measuring the temperature difference of the two bodies. Therefore the detector will be designed to cool through conduction. Here it will be proven that the amount of conduction from the bodies to the surroundings and from body to body can be determined with the difference in temperature between the two bodies.
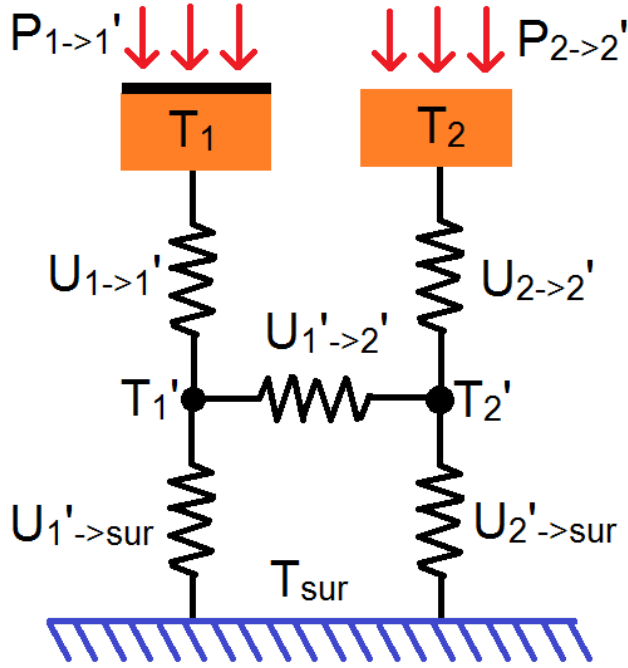
The conduction diagram is shown in *Figure 15*.

Figure 15: Schematic representation of the conduction system leading the incoming power fluxes $P_{1\to1'}$ and $P_{2\to2'}$ to the surroundings with temperature T_{sur}. This results in the temperatures T_1 and T_2 in the bodies and T_1' and T_2' in the junctions that are connected.

The power balances of the two bodies 1 and 2 and the junctions 1' and 2' are

$$P_{1\to1'} = nV + \alpha_1 pS - \varepsilon_1 \sigma S(T_1^4 - T_{sur}^4) - \rho cV \frac{dT_1}{dt}, \tag{5.6}$$

$$P_{2\to2'} = nV + \alpha_2 pS - \varepsilon_2 \sigma S(T_2^4 - T_{sur}^4) - \rho cV \frac{dT_2}{dt}, \tag{5.7}$$

$$P_{1\to1'} = P_{1'\to sur} + P_{1'\to2'}, \quad P_{2\to2'} = P_{2'\to sur} - P_{1'\to2'}. \tag{5.8}$$

The relations between conducted power $P_{i\to j}$ and temperature difference $T_i - T_j$ are linear, characterized by an overall heat transfer coefficient $U_{i\to j}$. This is shown in *Appendix C*. In order to simplify the analysis and the result several equivalent quantities are introduced

$$\Delta T = T_1 - T_2, \quad \Delta T' = T_1' - T_2', \quad \Delta P = P_{1\to1'} - P_{2\to2'}, \quad \Delta P' = P_{1'\to sur} - P_{2'\to sur}, \tag{5.9}$$

More equivalent quantities can be introduced when the following is assumed. Body 1 is absorbs more microwave radiation power than body 2 ($\alpha_1 > \alpha_2$) in order to get a net measurement. Body 1 has a higher emissivity than body 2 ($\varepsilon_1 > \varepsilon_2$) which allows the definition of the following quantities

$$\alpha = \alpha_1 - \alpha_2, \quad \varepsilon = \frac{\varepsilon_1 T_1^4 - \varepsilon_2 T_2^4 - (\varepsilon_1 - \varepsilon_2)T_{sur}^4}{T_1^4 - T_2^4} \approx \varepsilon_1. \tag{5.10}$$

Note that ε is slightly temperature dependent, except when $\varepsilon_1 = \varepsilon_2$, but this is negligible. Further simplification is possible when assuming that

$$U^* = U_{1\rightarrow 1'} = U_{2\rightarrow 2'}, \quad U' = U_{1'\rightarrow sur} = U_{2'\rightarrow sur}, \tag{5.11}$$

which is true when the conduction is symmetric. This is an important design consideration. The analysis of the power balance is given in *Appendix C*. An equivalent overall heat transfer coefficient U_{eq} is now introduced

$$U_{eq} = \frac{U^*(U' + 2U_{1'\rightarrow 2'})}{U^* + U' + 2U_{1'\rightarrow 2'}}, \tag{5.12}$$

which results in the following power balance difference

$$\rho c V \frac{d\Delta T}{dt} = \alpha p S - \left[U_{eq} + \varepsilon \sigma S (T_1 + T_2)(T_1^2 + T_2^2) \right] \Delta T. \tag{5.13}$$

The relative error made by neglecting the fact that radiation scales with the power of four instead of linearly with the temperature difference ΔT is

$$e_r = \frac{\varepsilon \sigma S}{U_{eq}} (T_1 + T_2)(T_1^2 + T_2^2). \tag{5.14}$$

This depends approximately (because of the temperature dependent ε) on the absolute temperature with the power of three instead of four because the radiation is assumed to be conductive. Rewriting equation (5.13) excluding the unresolvable radiation error term gives

$$\alpha p S = \rho c V \frac{d\Delta T}{dt} + U_{eq} \Delta T. \tag{5.15}$$

This equation is similar in form to the Wendelstein-7X bolometer of equation (4.12), except that it depends on a temperature difference ΔT instead of the absolute temperature T. When assuming the microwave power density p to be constant this differential equation can be solved

$$\Delta T(t) = \left(\frac{\alpha p S}{U_{eq}} - \Delta T_0 \right) \left[1 - \exp\left(-\frac{U_{eq}}{\rho c V}(t - t_0) \right) \right] + \Delta T_0, \tag{5.16}$$

where $\Delta T(t = t_0) = \Delta T_0$ is the initial temperature difference at the initial time t_0. This function is an exponential decay to the temperature difference $\alpha p S / U_{eq}$ with a characteristic time $\rho c V / U_{eq}$.

6. Design

Now that the relation between the microwave power density and the difference in temperature is established the detector can be designed. An attempt has been made to make the detector as sensitive as possible while designing simple and cost effective as well as being conservative in modifications to the junction box. First the conceptual design is discussed to give a basic idea of the layout of the components in the detector. Secondly the requirements of *Chapter 2* and the design considerations found in *Chapter 5* are combined to yield the detector criteria. These are then used to design the solid bodies. This results in a requirement for the conduction system which in turn results in a requirement on the bolt and disc spring system. Two different bolt and disc spring systems are discussed and an assessment is made on the error in determining the microwave power density. After this the differential thermocouple and the isothermal block are designed. The isothermal block can also be left out however but this will also create an error. Finally the modifications to the junction box are summarized. An analysis of all possible error sources that have been encountered is given in *Appendix E*. This provides a basis for recommending the design choices. A list of specifications of the detector is given in *Appendix D*.

Conceptual design

The conceptual design of the modified junction box capable of housing the microwave detector is shown in *Figure 16*.
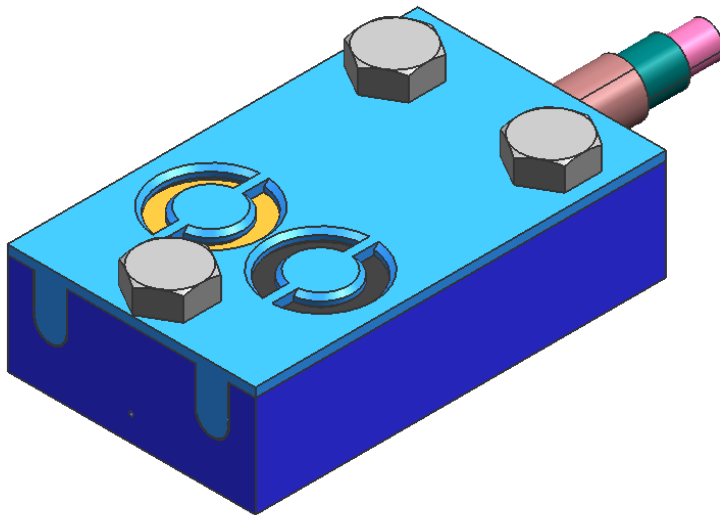
Figure 16: Isometric view of the microwave detector. The dimensions are roughly 45x27x13 mm.

The original two cables entering from the back are replaced by plugs fitted on the lid. The microwaves that will be used to determine the microwave power density come in from the top through a hole in the lid where they are either absorbed or reflected by a coated (black) or bare (orange) cylinder. This microwave power will heat up the cylinders, one more so than the other.

When the lid (light blue) and the bolts (grey) that fix the lid are hidden the interior of the detector is visible. This is shown in *Figure 17*.
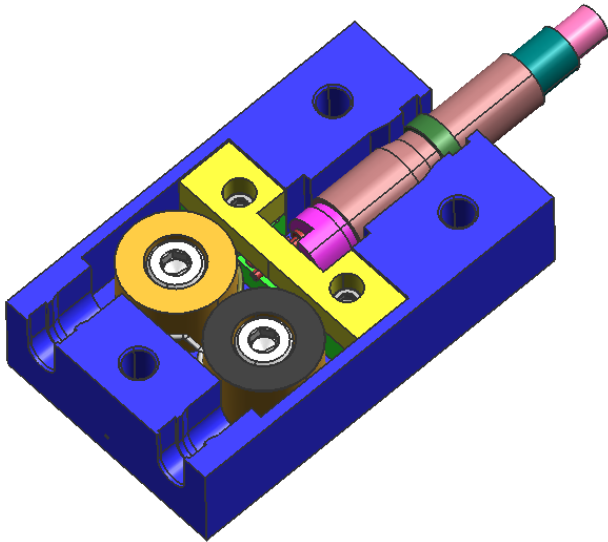
Figure 17: View of the microwave detector. The lid and the bolts connecting the lid are hidden. The interior is now visible.

It is now visible that the cylinders are bolted (light grey) to the junction box base (dark blue) to conduct the generated heat away. Also the two electrically insulating support structures for the differential thermocouple wire are visible. The bottom one serves as the isothermal block (light green) for the thermocouple wire and the cable wire, and the top one (yellow) is simply present to keep the wires in place. This is better visible from top view when the top support structure is also hidden as is shown in *Figure 18*.
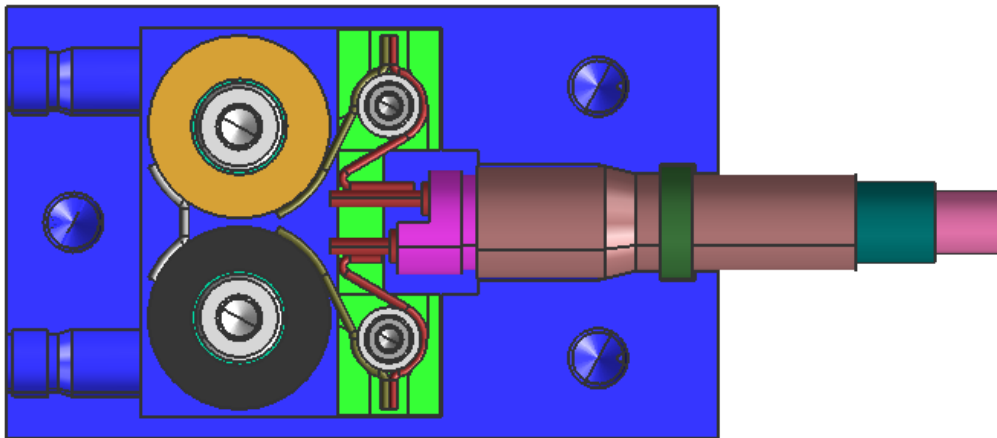
Figure 18: Top view of the microwave detector. The lid, the bolts fastening it and the top support structure are hidden. The electrical system is now visible.

Now two additional bolts (grey) are visible. These bolts serve a double purpose. First they fix the bottom support to the junction box base and secondly they keep a small electrically insulating washer (light grey) in place that is used to clamp the thermocouple wire (brown) and the cable wire (red) for thermal contact. Finally for a view of the conduction system a vertical slice through the axes of the cylinders is shown in *Figure 19*.

Figure 19: Slice through the axes of the cylinders. This shows the symmetry of the two cylinders.

In this figure the thermal path for the conduction is visible. Heat is generated by the absorbed microwaves and neutron radiation will increase the temperature i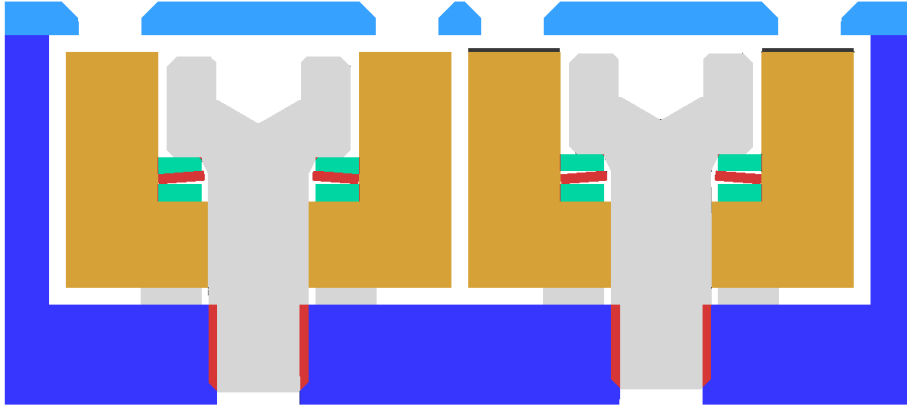n the cylinders. As the temperature increases the cylinders will expand. If this is constrained then this will increase the pressure which will increase the thermal contact of the cylinder with the junction box base. This will increase conduction by an unknown amount and this will result in an error in determining the power density or worse if the bolt fails. To avoid this disc springs (red) are placed below the head of the bolt to ensure constant pressure and thus constant conduction. The heat is then conducted away through an electrically insulating washer (light grey) to the junction box base and then to the vacuum vessel through the welds on the sides of the base. To prevent peak stresses in the copper and in the bolt, flat washers (blue green) are placed below and above the disc spring.

Detector criteria
From the requirements of *Chapter 2* the design criteria for the solid bodies can be derived. First of all the Biot number Bi should be lower than 0.1 to validate the use of the lumped capacitance method

$$Bi = \frac{L_c}{k_{int}} \left| \frac{\alpha p}{T - T_{sur}} - \varepsilon\sigma(T_{max} + T_{sur})(T_{max}^2 + T_{sur}^2) + \frac{U}{A} \right| < 0.1, \tag{6.1}$$

where U is defined as $U = P_{1\rightarrow 1'}/(T - T_{sur})$. Secondly the response time τ should be much smaller than the minimum integration time of $t_{int} = 5$ s to make sure that the temperature is uniformly distributed well within the integration period so that the measurement represents the average temperature of the body

$$\tau = \frac{\rho c L_c^2}{k_{int}} \ll t_{int}. \tag{6.2}$$

For the other criteria a maximum temperature T_{max} has to be defined. The lowest limitation to the temperature is the disc spring. Even with the special high temperature precipitation hardening iron base super-alloy A286[15] the maximum working temperature is $T_{max} = 816\,°C$. This is explained later. The initial temperature is considered to be the surrounding temperature which is around $T_{sur} = 100\,°C$.

Only the coated body (body 1) is considered for reaching this maximum temperature. The power balance of equation (3.19) is used to find the appropriate criteria. Neutron radiation nV is negligible when the maximum power densities αpS are considered and heat radiation $\varepsilon \sigma S(T^4 - T_{sur}^4)$ can also be neglected as this should be relatively low. First startup is considered. This is expected to take a maximum of $t_{start} = 5.5$ s with a power density $p_{start} = 3$ MW/m². During this phase conduction losses $U(T - T_{sur})$ will be negligible and only thermal inertia $\rho cV dT/dt$ can avoid overheating

$$\rho cV \frac{dT}{dt} = \alpha pS. \tag{6.3}$$

This differential equation can be solved to yield the startup criterion

$$\frac{\alpha S}{\rho cV} < \frac{T_{max} - T_{sur}}{p_{start} t_{start}}. \tag{6.4}$$

Equation (6.3) can also be used to define the transient sensitivity of the detector in terms of a temperature difference ΔT

$$\frac{1}{p} \frac{d\Delta T}{dt} = \frac{\alpha S}{\rho cV}, \tag{6.5}$$

or in terms of a voltage ΔV

$$\frac{1}{p} \frac{d\Delta V}{dt} = \frac{S_A - S_B}{p} \frac{d\Delta T}{dt} = \frac{(S_A - S_B)\alpha S}{\rho cV}, \tag{6.6}$$

where $S_A - S_B$ is the difference in Seebeck coefficients.

Now steady state is considered with a power density $p_{sts} = 1.25$ MW/m². In this phase the transient $\rho cV dT/dt$ is absent and only conduction can prevent overheating

$$U(T - T_{sur}) = \alpha pS. \tag{6.7}$$

Rewriting gives the steady state criterion

$$\frac{\alpha S}{U} < \frac{T_{max} - T_{sur}}{p_{sts}}. \tag{6.8}$$

Equation (6.7) can now in the same manner as equation (6.5) be used to define the steady state sensitivity of the detector both in terms of a temperature difference ΔT and in terms of a voltage ΔV

$$\frac{\Delta T}{p} = \frac{\alpha S}{U}, \tag{6.9}$$

$$\frac{\Delta V}{p} = (S_A - S_B)\frac{\Delta T}{p} = \frac{(S_A - S_B)\alpha S}{U}. \tag{6.10}$$

The final design criterion is that of the maximum error for both the maximum and the minimum microwave power. The total error of all error sources combined should be lower than the maximum allowable error

$$e_{tot} = \sum_i e_i < e_{max}. \tag{6.11}$$

When this is true the error in between the maximum and minimum power is assumed to be lower than either of these. One intrinsic material error is that of the specific heat capacity c of the transient term. The error can be determined by dividing the difference in specific heat capacity c at the surrounding and maximum temperature by the assumed specific heat capacity, at the surrounding temperature

$$e_c = \frac{|c(T_{max}) - c(T_{sur})|}{c(T_{sur})}. \tag{6.12}$$

The same argument goes for the equivalent overall heat transfer coefficient U_{eq} in the steady state term

$$e_U = \frac{|U_{eq}(T_{max}) - U_{eq}(T_{sur})|}{U_{eq}(T_{sur})}. \tag{6.13}$$

The final two errors are significant only for the minimum power density of $p = 0.5$ kW/m^2 with an integration time $t_{int} = 60$ s. The problem here is the electromagnetic interference in the vessel. No thorough investigation has been done but according to an expert the main source of interference is the changing magnetic field. The integral law of Faraday gives the interference voltage V_{int}

$$V_{int} = \frac{dB}{dt}O, \tag{6.14}$$

where dB/dt is the time derivative of the magnetic field in the direction of the open loop of the differential thermocouple and O is the area of this loop. This voltage by itself may not be very large but it can have a high frequency which makes differentiation difficult. Without differentiation no time dependent analysis can be done and the system needs to be in steady state. The error that is produced by not being completely in steady state is

$$e_t = \exp\left(-\frac{U_{eq}}{\rho c V}t_{int}\right). \tag{6.15}$$

In steady state the temperature difference ΔT is a direct linear function of the power density p

$$\Delta T = \frac{\alpha p S}{U_{eq}}, \tag{6.16}$$

and this produces a voltage according to equation (5.2)

$$\Delta V = (S_A - S_B)(T_2 - T_1) = (S_A - S_B)\Delta T = (S_A - S_B)\frac{\alpha p S}{U_{eq}}. \tag{6.17}$$

To reduce the noise of the electromagnetic interference it is averaged out. The voltage error that is left can be determined with the root of N law[16], where N is the number of measurements that is averaged over. If the integration time is t_{int} and the sample time is t_s then the interference voltage is

$$V_{int} = \frac{dB}{dt}O/\sqrt{N} = \frac{dB}{dt}O/\sqrt{t_{int}/t_s}. \tag{6.18}$$

The error caused by this interference voltage is the ratio of the interference voltage over the thermo-electric voltage

$$e_V = \frac{V_{int}}{\Delta V} = \frac{U_{eq}\frac{dB}{dt}O}{(S_A - S_B)\alpha p S \sqrt{t_{int}/t_s}}. \tag{6.19}$$

All criteria for the solid bodies are summarized in *Table 3*.

Table 3: Summary of the design criteria for the solid body cylinders.

Description	Criterion
Lumped capacitance validity	$Bi = \dfrac{L_c}{k_{int}}\left\|\dfrac{\alpha p}{T - T_{sur}} - \varepsilon\sigma(T_{max} + T_{sur})(T_{max}^2 + T_{sur}^2) + \dfrac{U}{A}\right\| < 0.1$
Minimum integration time	$\tau = \dfrac{\rho c L_c^2}{k_{int}} \ll t_{int}$
Minimum thermal inertia	$\dfrac{\alpha S}{\rho c V} < \dfrac{T_{max} - T_{sur}}{p_{start}t_{start}}$
Minimum conduction cooling	$\dfrac{\alpha S}{U} < \dfrac{T_{max} - T_{sur}}{p_{sts}}$
Maximum error	$e_{tot} = \displaystyle\sum_i e_i < e_{max}$

Solid body cylinders

The material for the solid bodies are preferably thermally as well as electrically conductive so that the differential thermocouple can be attached at any point which simplifies the design and creates a better defined electrical path. This is tested in an experiment in *Chapter 7*. For thermal and electrical conductivity the best materials are pure metals. The metals with the highest thermal conductivity are silver, copper, gold and aluminum. For economic purposes and transmutation due to neutron radiation only copper and aluminum are considered. The melting temperature of aluminum is 660 °C which is below the maximum working temperature of the disc springs. Therefore copper is preferred. The properties of copper are given in *Table 4*.

Table 4: Properties of copper under the specified neutron irradiation.

Variable	Symbol	Value
Internal thermal conductivity	k_{int}	390 W/mK
Emissivity	ε_2	0.03
Microwave absorption coefficient	α_2	0.01
Density of body	ρ	8960 kg/m^3
Specific heat capacity at surrounding temperature	$c(100\ °C)$	395 J/kgK
Specific heat capacity at maximum temperature	$c(816\ °C)$	463 J/kgK
Neutron power density	n	0.4 W/cm^3

As the ratio of volume over surface $L_c = V/S = 12$ mm is practically defined by the height of the junction box and the material is known the maximum microwave absorption coefficient α can be determined with the startup criterion of equation (6.4) as $\alpha = 1.8$. An absorption coefficient higher than one is obviously impossible and a coating material should be used which has an absorption coefficient that is as high as possible. One ceramic coating with a very high absorption coefficient has been found and tested in the MISTRAL[11]. This ceramic coating is a mixture of alumina and titania (Al_2O_3-TiO_2). For the wavelength of 2.14 mm used in the MISTRAL the absorption coefficient is $\alpha_1 = 0.81$. This is assumed to be the same for the ITER wavelength of 1.76 mm. The emissivity of this material is also very high $\varepsilon_1 = 0.9$. This means that radiation losses will be dominated by this coating alone. The sensitivity of the detector can now also be calculated and is $d\Delta T/dt/p = 1.93 \cdot 10^{-5}$ Km^2/J or $d\Delta V/dt/p = 7.91 \cdot 10^{-10}$ Vm^2/J for the transient term and $\Delta T/p = 5.65 \cdot 10^{-4}$ Km^2/W or $\Delta V/p = 2.32 \cdot 10^{-8}$ Vm^2/W for the steady state term.

The error in the transient term caused by the non-constant specific heat capacity c can now be evaluated with equation (6.12) and is $e_c = 17$ %. This is within the acceptable limits but only a small margin of 3 % remains for all other errors in the transient term.

With the ratio of volume over surface L_c set, the typical thermal response time can be calculated with equation (6.2) $\tau = 1.3$ s. So for an integration time of $t_{int} = 5$ s the Fourier number is $Fo = 4$. This fulfills the criterion for the thermal response time.

The exposed surface of the cylinder is $S = 48$ mm^2 and the volume is $V = 579$ mm^3. This can be used to calculate the overall heat transfer coefficient of conduction that is required with the criterion of equation (6.8) as $U = 0.068$ W/K.

Now the Biot number can be calculated with equation (6.1). For steady state the maximum Biot number is $Bi = 0.08$ which is only just lower than the critical value of 0.1. For the startup phase the Biot number is $Bi = 0.15$ which is above the critical value. This means that the temperature in the cylinder cannot be assumed uniform. So the place where the thermocouples are attached is important in this case. The cylinders are axisymmetric so the only direction of the gradient in temperature can be vertical or radial. So to measure the average temperature the thermocouples should be connected at approximately half the height of the cylinder.

The equivalent overall heat transfer coefficient is calculated in the next paragraph as $U_{eq} = 0.072$ W/K. Now the error due to radiation can be calculated with equation (5.14) as $e_r = 7$ %. This is well below the maximum acceptable error $e_{max} = 20$ % and as will be shown later the overall heat transfer coefficient U decreases with temperature so this will counteract the extra losses due to radiation.

The final set of errors is specific for the measurement of the minimum power density. First the error due to not being in steady state is analyzed. The characteristic time of the exponential decay is $\rho c V / U_{eq} = 29$ s and the integration time is $t_{int} = 60$ s. This is not much longer so with equation (6.15) the non-steady state error is calculated as $e_t = 13$ %. This has to be added to the error caused by the electromagnetic interference. The area of the closed loop with the normal in the radial direction is determined as $O = 88$ mm^2 and the time derivative of the magnetic field in radial direction under normal operation is $dB/dt = 0.1$ T/s. The difference in the Seebeck coefficients is assumed to be $S_A - S_B = 41$ µV/K. With a sample time $t_s = 100$ ms and an integration time $t_{int} = 60$ s the error due to magnetic interference is calculated with equation (6.19) and reduces to $e_V = 3$ %. Added to the non-steady state error this gives a total error of 16 % which is below the maximum error of $e_{max} = 20$ % so it is acceptable.

Conduction system

Previously the heat conduction through the washer connecting the cylinder and the base was assumed to be critical for the heat transfer. For a more detailed requirement on this washer conduction U_{wash} the base is analyzed first. The base is made from stainless steel 316L. The heat that is conducted through the washer will enter the base from the top. In order to be conducted through the bottom base plate it first has to travel vertically. On average it will have to reach the mid-plane $H/2$ of the base plate. This is shown in *Figure 20*.

Figure 20: Vertical conduction system of the microwave detector. In red is the direction of the heat conduction from the conducting washers to the mid-plane of the junction box base. The dimensions given are characteristic for the system.

The total overall heat conduction coefficient U^* from the cylinder to the mid-plane then becomes

$$U^* = \frac{1}{\frac{1}{U_{wash}} + \frac{2H}{\pi k(D^2 - d^2)}},$$ (6.20)

or for the washer overall heat conduction coefficient U_{wash}

$$U_{wash} = \frac{1}{\frac{1}{U^*} - \frac{2H}{\pi k(D^2 - d^2)}},$$ (6.21)

where D and d are the outer and inner diameter of the washer respectively.

From this mid-plane the heat can travel to either to the vacuum vessel through the welds at the edges of the base or to the other cylinder. This is shown in *Figure 21*.
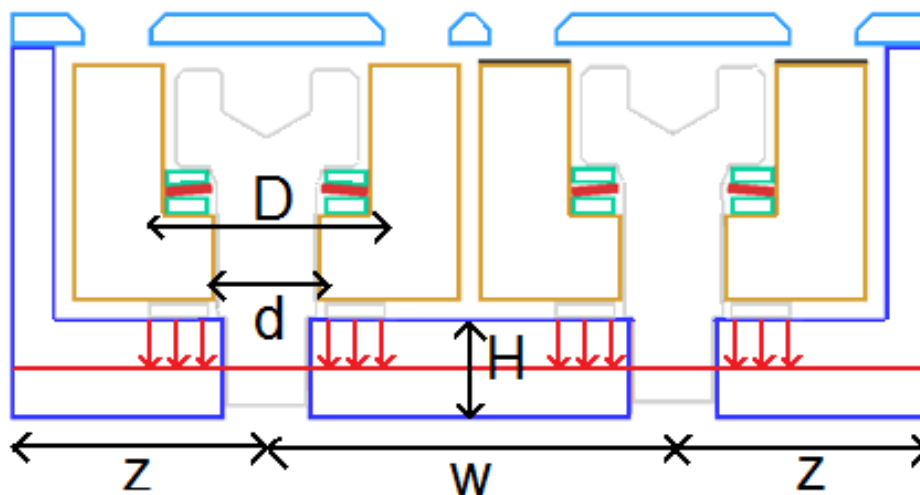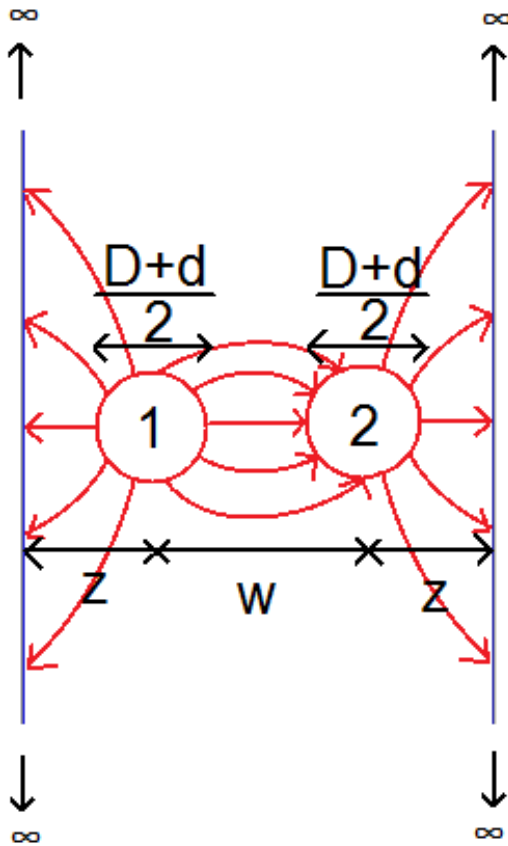

Figure 21: Horizontal conduction system of the microwave detector. In red is the direction of the heat conduction through the mid-plane of the junction box base. Conduction is possible from washers to the edge or from washer to washer. The dimensions given are characteristic for the system.

The heat conduction from a cylinder to the edge of the base is represented by a horizontal isothermal cylinder of length H buried in a semi-infinite medium. The diameter of this isothermal cylinder is chosen to be the average of the inner and outer diameter of the washer $(D + d)/2$. The distance from the center of the cylinder to the edge is z. The overall heat transfer coefficient from the cylinder to the surroundings is[10]

$$U' = \frac{2\pi k H}{\ln\left(\frac{8z}{D + d}\right)}.$$

(6.22)

The heat conduction from one cylinder to the other is represented by conduction between two cylinders of length H in infinite medium. The distance between the centers of the cylinders is w. The overall heat transfer coefficient from cylinder to cylinder is[10]

$$U_{1'\to2'} = \frac{2\pi k H}{\text{arccosh}\left(\frac{8w^2}{(D + d)^2} - 1\right)}.$$

(6.23)

To determine the overall heat transfer coefficient through the washer U_{wash} first the boundary conditions of the conduction system of *Figure 15* are analyzed. For body 1 the power $P_{1\to1'}$ that is to be conducted away from the body can be found by evaluating the power balance in steady state at the maximum temperature

$$P_{1\to1'} = \alpha_1 pS + nV - \varepsilon\sigma S(T_{max}^4 - T_{sur}^4).$$

(6.24)

For body 2 temperatures will always be relatively low so radiation losses can be neglected

$$P_{2\to2'} = \alpha_2 pS + nV.$$

(6.25)

The relevant dimensions and the thermal conduction coefficient k of the stainless steel base are given in *Table 5*.

Table 5: Properties and dimensions of the junction box base and the conducting washers.

Variable	Symbol	Value
Thermal conduction coefficient base	k	15.5 W/mK
Height of base plate	H	2.975 mm
Outer diameter	D	7.00 mm
Inner diameter	d	3.38 mm
Distance from cylinder center to edge	z	7.525 mm
Distance between cylinder centers	w	11.95 mm

Equations (5.8) substituted with equations (C.1-C.3) and equations (5.11) give

$$P_{1\to1'} = U^*(T_1 - T_1') = U'(T_1' - T_{sur}) + U_{1'\to2'}(T_1' - T_2'),$$

(6.26)

$$P_{2\to2'} = U^*(T_2 - T_2') = U'(T_2' - T_{sur}) - U_{1'\to2'}(T_1' - T_2').$$

(6.27)

These four independent equations can be solved for the unknown variables U^*, T_2, T_1' and T_2'. Only the overall heat transfer coefficient U^* is given here

$$U^* = \frac{P_{1\to1'}U'(U' + 2U_{1'\to2'})}{U'(U' + 2U_{1'\to2'})(T_1 - T_{sur}) - P_{1\to1'}(U' + U_{1'\to2'}) - P_{2\to2'}U_{1'\to2'}}, \qquad (6.28)$$

the equations for the other variables can be found in *Appendix C*. Now all variables that are necessary to determine the overall heat transfer coefficient U_{wash} are known and given in *Table 6*.

Table 6: Parameters of the conduction system.

Variable	Symbol	Value
Power to be conducted away from body 1	$P_{1\to1'}$	45.4 W
Power to be conducted away from body 2	$P_{2\to2'}$	0.83 W
Surrounding temperature	T_{sur}	100 °C
Temperature in mid-plane base below body 1	T_1'	307 °C
Temperature in mid-plane base below body 2	T_2'	182 °C
Temperature in body 1	T_1	816 °C
Temperature in body 2	T_2	191 °C
Heat transfer coefficient from cylinder to edge	U'	0.16 W/K
Heat transfer coefficient from cylinder to cylinder	$U_{1'\to2'}$	0.098 W/K
Heat transfer coefficient from body to surroundings	U	0.063 W/K
Heat transfer coefficient from body to mid-plane base	$U^*(100 \degree C)$	0.091 W/K
Equivalent heat transfer coefficient	$U_{eq}(100 \degree C)$	0.072 W/K
Washer overall heat transfer coefficient	$U_{wash}(100 \degree C)$	0.13 W/K

Compared to the overall heat transfer coefficients of the base U' the overall heat transfer coefficient of the washer U_{wash} is similar. This means that the thermal conduction through the washer should be designed to be almost as good as the thermal conduction through the base. The thermal conduction through the washer U_{wash} consists of two thermal contacts, one from cylinder to washer $U_{c\to w}$ and one from washer to base $U_{w\to b}$, and the conduction through the washer itself U_w. The conduction through the washer is

$$U_w = \frac{\pi k_w (D^2 - d^2)}{4t}, \qquad (6.29)$$

where k_w is the thermal conductivity of the washer and t is the thickness of the washer. Contact conduction U_{cont} between two materials A and B can be described with the following empirical formula[17]

$$U_{cont} = \frac{2.5k_Ak_B}{k_A + k_B}\left(\frac{76}{\sqrt{\sigma_s}}\right)\frac{F}{3.178 \cdot 10^9(4.0 - 1.8H_G)\left(2.1 \cdot 10^4\sqrt{\sigma}\right)^{-0.57+0.26H_G}}, \qquad (6.30)$$

where F is the force that is applied to the contact in Newtons (N), H_G is the macroscopic hardness of the softer of the two materials in GigaPascal (GPa), σ is the surface roughness of the harder of the two materials in meters (m) and σ_s is the RMS surface roughness of the two contact planes defined as

$$\sigma_s = \sqrt{\sigma_A^2 + \sigma_B^2}, \tag{6.31}$$

where σ_A and σ_B are the surface roughnesses of the two contact planes. This formula depends on only one variable, namely the force F, and the rest is captured in one constant C set by the material and manufacturing method. The formula is therefore simplified to

$$U_{cont} = CF \wedge C = \frac{2.5 k_A k_B}{k_A + k_B}\left(\frac{76}{\sqrt{\sigma_s}}\right)\frac{1}{3.178 \cdot 10^9 (4.0 - 1.8H_G)\left(2.1 \cdot 10^4 \sqrt{\sigma}\right)^{-0.57 + 0.26 H_G}}. \tag{6.32}$$

The washer material should be chosen such that the force F applied by the bolt does not cause the bolt to fail. The only economical material that is electrically insulating, has a high thermal conductivity k_w and is neutron and vacuum compatible is aluminum nitride (AlN). It should be noted however that under neutron irradiation the thermal conductivity k_w will degrade slowly over time, but this should not be a problem since the detector will be shielded from the highest power densities by the blankets as soon as neutrons will be produced. The cylinder and the base are assumed to have the same roughness. The constants C are calculated and shown in *Table 7*.

Table 7: Parameters of the conducting washers and their contact with the copper cylinders and junction box base.

Variable	Symbol	Value
Thermal conductivity washer	k_w	180 W/mK
Thickness washer	t	0.5 mm
Macroscopic hardness cylinder	$H_{G,c}$	0.61 GPa
Macroscopic hardness base	$H_{G,b}$	1.4 GPa
Surface roughness metals	σ_m	10 µm
Surface roughness ceramic	σ_w	30 µm
RMS surface roughness	σ_s	32 µm
Material constant cylinder to washer	$C_{c \to w}$	2.52 mW/KN
Material constant washer to base	$C_{w \to b}$	0.24 mW/KN

The total washer conduction can be written as a function of the force

$$U_{wash} = \frac{1}{\frac{1}{U_{c \to w}} + \frac{1}{U_w} + \frac{1}{U_{w \to b}}} = \frac{1}{\frac{1}{F}\left(\frac{1}{C_{c \to w}} + \frac{1}{K C_{w \to b}}\right) + \frac{4t}{\pi k_w (D^2 - d^2)}}, \tag{6.33}$$

where K is a factor that can be applied to account for an increase in the conductivity between the washer and the base. This is used later on. An explicit formula for the required force F can now be deducted

$$F = \frac{\frac{1}{C_{c \to w}} + \frac{1}{K C_{w \to b}}}{\frac{1}{U_{wash}} - \frac{4t}{\pi k_w (D^2 - d^2)}}. \tag{6.34}$$

Without an increase in conductivity between the washer and the base the factor is $K = 1$. The required force to provide the necessary conduction is calculated as $F = 601$ N. This will be provided by the bolt.

Bolt and disc spring

The maximum force F_{max} that a bolt can apply depends on the torque to destruction T_{des} that can be applied before failure. As the bolt should also electrically insulate the cylinder from the junction box base a ceramic insulator is necessary. The simplest choice is to use an M3x7 alumina socket head screw, but this has some disadvantages. First it should be fastened inside the stainless steel base. After the correct torque is applied and the conduction is optimal a droplet of glue of about a cubic millimeter should be applied to the bottom of the bolt and the edges of the hole. The inorganic adhesive Thermoguss 2000[18] should be able to do the job. It has a maximum temperature of 1093 °C, well above the maximum temperature of the disc springs, it glues to both ceramics and metals and it is vacuum and neutron irradiation compatible. Secondly the bolt will require a tensile loading of the ceramic, which is a weakness of ceramic. So for these purposes a stainless steel M2x8 socket head screw is also investigated with a ceramic cover around it. This bolt is easily fixed into place with a small weld on the bottom of the bolt. The bolt with the ceramic cover is shown in purple in *Figure 22*.
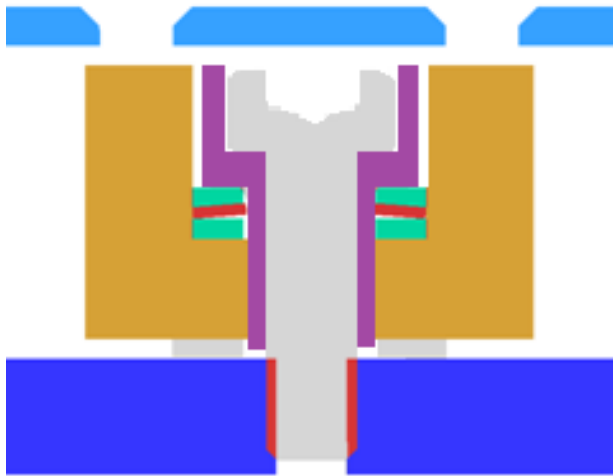
Figure 22: Slice through the axis of one of the cylinders. Instead of the ceramic M3x7 bolt a stainless steel M2x8 bolt is used with a ceramic cover around it.

The relation between the maximum allowable force F_{max} and the torque to destruction T_{des} is

$$F_{max} = \frac{2T_{des}}{Sfd},$$
(6.35)

where S is the safety factor, f is the friction factor and d is the diameter of the thread bolt. A safety factor $S = 2$ is applied to allow for some imperfections of the bolt and some room for calibrating the conduction.

The rest of the parameters are given in *Table 8*.

Table 8: Parameters of the two different bolt types and their connection with the surroundings.

Variable	Symbol	Alumina M3x7	Stainless steel M2x8
Thread diameter of bolt	d	3 mm	2 mm
Destructive torque	T_{des}	0.6 Nm	0.8 Nm
Friction factor	f	0.5	0.5
Safety factor	S	2	2
Maximum force	F_{max}	400 N	800 N

This shows that only the stainless steel bolt can provide a sufficient force F for the conduction. However a copper foil between the washer and the base has been reported to be able to increase the thermal conduction $U_{w \to b}$ by a factor of $K = 3$[17] which results in a required force of only $F = 235$ N. This is well below the maximum force $F_{max} = 400$ N that can be provided safely with the ceramic bolt.

Now the only thing that remains is to find a disc spring that can keep the force F as constant as possible over the entire temperature range in which the detector can operate. The dimensions d, D, h and t of the disc spring are shown in *Figure 23*.
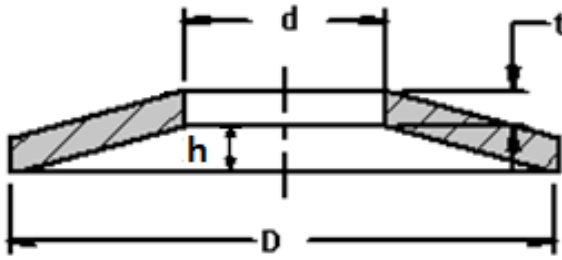
Figure 23: Cross-section of a disc spring. The dimensions are characteristic for the spring.

The maximum force F_{max} that a disc spring can take while still working as a spring is[19]

$$F_{max} = \frac{4Et^3 h}{S(1 - \mu^2)\gamma D^2},$$ (6.36)

where E is the modulus of elasticity and μ is the lateral contraction coefficient. The safety factor S is added to the equation to make sure that the bolt will fail at the same time the disc spring is flattened. The dimensionless numbers γ and δ are defined as[19]

$$\gamma = \frac{1}{\pi} \frac{\left(\frac{\delta - 1}{\delta}\right)^2}{\frac{\delta + 1}{\delta - 1} - \frac{2}{\ln(\delta)}} \quad \wedge \quad \delta = D/d.$$ (6.37)

Rewriting equation (6.36) gives an explicit expression for the thickness t for a given height to thickness ratio β

$$t = \sqrt[4]{\frac{F_{max}S(1-\mu^2)\gamma D^2}{4E\beta}} \quad \wedge \quad \beta = h/t. \tag{6.38}$$

The inner d and outer D diameters of the spring are set by the dimensions of the bolt. The height to thickness ratio β is chosen low for linear spring characteristics. The values for these parameters and their derived parameters are given in *Table 9*.

Table 9: Parameters of the disc springs.

Variable	Symbol	Value
Inner diameter	d	3.2 mm
Outer diameter	D	6 mm
Height to thickness ratio	β	0.4
Diameter ratio	δ	1.875
Shape constant	γ	0.666
Modulus of elasticity at surrounding temperature	$E(100\ °C)$	199 GPa
Lateral contraction coefficient	μ	0.3
Safety factor	S	2

For the alumina bolt the thickness t and the height h of the disc spring can now be calculated as 0.5 mm and 0.2 mm respectively. For the stainless steel bolt these values are 0.6 mm and 0.24 mm. The equation for the force F as a function of the indentation s of the spring is[19]

$$F(s,T) = \frac{4E(T)t^4}{(1-\mu^2)\gamma D^2}\frac{s}{t}\left[\left(\frac{h}{t}-\frac{s}{t}\right)\left(\frac{h}{t}-\frac{s}{2t}\right)+1\right]. \tag{6.39}$$

The indentation s cannot be explicitly expressed so this equation is solved numerically. The indentions s for the alumina and stainless steel bolts are respectively 0.05 mm and 0.07 mm. The increase of this indentation Δs is due to thermal expansion and can be calculated by adding all thermal expansions from the base of the junction box to the head of the bolt and subtracting that with the thermal expansion of the bolt. The formula for this is as follows

$$\Delta s = \Delta T \sum_i \alpha_i l_i, \tag{6.40}$$

where ΔT is the difference between the maximum temperature T_{max} and the surrounding temperature T_{sur}. α_i and l_i are respectively the thermal expansion coefficients and lengths of the different materials i.

Table 10 shows the parameters used to calculate the thermal expansion Δs to obtain the resulting force F and overall heat transfer coefficient U_{eq} at the maximum temperature T_{max}.

Table 10: Parameters of the thermal expansion from the junction box base up to the head of the bolt for the two different types of bolts.

Variable	Symbol	Alumina M3x7	Stainless steel M2x8
Expansion coefficient copper	α_{Cu}	16.6 µm/mK	16.6 µm/mK
Expansion coefficient conducting washer	α_w	4.5 µm/mK	4.5 µm/mK
Expansion coefficient disc spring	α_{spring}	16.5 µm/mK	16.5 µm/mK
Expansion coefficient spring washers	$\alpha_{washers}$	16 µm/mK	16 µm/mK
Expansion coefficient ceramic cover	α_{cover}	0 µm/mK	8.1 µm/mK
Expansion coefficient bolt	α_{bolt}	8.1 µm/mK	16 µm/mK
Length copper	l_{Cu}	2.375 mm	2.255 mm
Length conducting washer	l_w	0.5 mm	0.5 mm
Length disc spring	l_{spring}	0.65 mm	0.77 mm
Length spring washers	$l_{washers}$	1 mm	1 mm
Length ceramic cover	l_{cover}	0 mm	1 mm
Length bolt	l_{bolt}	-4.525 mm	-5.525 mm
Thermal expansion per unit of temperature	$\sum_i \alpha_i l_i$	32 nm/K	-12 nm/K
Temperature difference	ΔT	716 °C	716 °C
Thermal expansion	Δs	23 µm	-9 µm
Modulus of elasticity at maximum temperature	$E(816\,°C)$	129 GPa	129 GPa
Force at maximum temperature	$F(816\,°C)$	217 N	340 N
Washer overall heat transfer coefficient	$U_{wash}(816\,°C)$	0.12 W/K	0.074 W/K
Heat transfer from body to mid-plane base	$U^*(816\,°C)$	0.086 W/K	0.060 W/K
Equivalent heat transfer coefficient	$U_{eq}(816\,°C)$	0.070 W/K	0.051 W/K

For the alumina bolt the increase in force due to thermal expansion Δs and the decrease in force due to the relaxation of the modulus of elasticity E approximately cancel each other out decreasing the force by only 18 N. For the stainless steel bolt the thermal expansion already relaxes the spring because of the high thermal expansion coefficient of stainless steel. Adding the relaxation of the modulus of elasticity causes a decrease in force of 261 N.

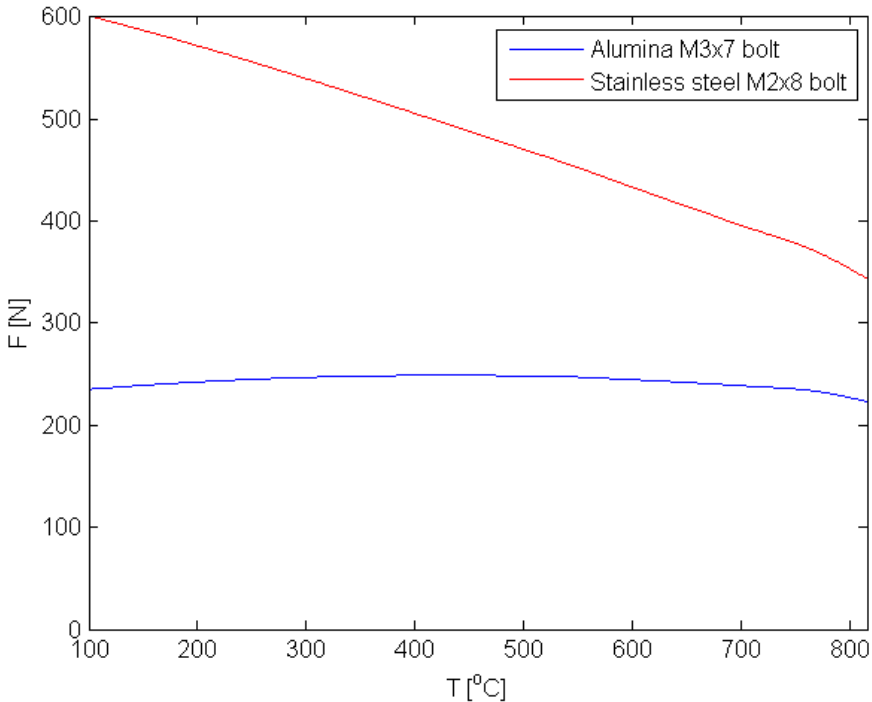This behavior is visualized in *Figure 24*[15].

Figure 24: Plot of the force provided by the bolt and disc spring against the temperature. In blue is the alumina M3x7 bolt and in red the stainless steel M2x8 bolt.

It should be noted that for the alumina bolt the difference between the maximum force that is reached and the force at the lowest temperature is smaller than the difference between the force at the maximum temperature and the force at the minimum temperature. The errors in determining the microwave power density p in steady state that are caused by the decrease in force F for the alumina and the stainless steel bolt e_U can be calculated with equation (6.13) and are respectively 4 % and 28 %. These errors however should not be added to the error caused by heat radiation e_r because they are of opposite sign. For the worst case the maximum absolute error should be taken. So for the alumina bolt the radiation error is highest creating an error of 7 %. For the stainless steel bolt the conduction error is highest creating an error of 28 %. This error is higher than the specified maximum error of $e_{max} = 20$ %. This means that with these specifications only the alumina bolt suffices.

Differential thermocouple

The differential thermocouple like a normal thermocouple consists of two different materials. These two materials should have a difference in Seebeck coefficients that is as constant as possible to ensure a minimum error in converting the voltage to a temperature difference. *Figure 25* shows the difference in Seebeck coefficients as a function of temperature for some standard thermocouple types.
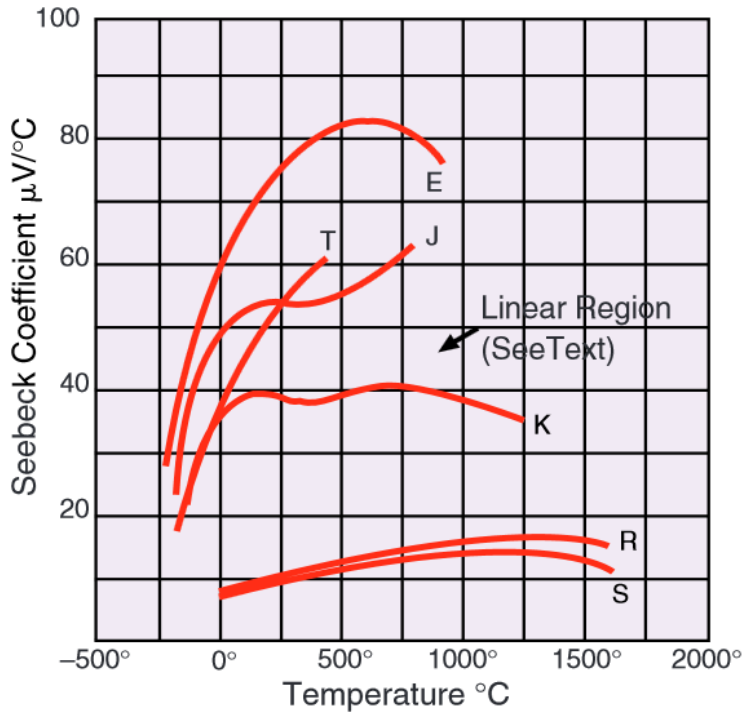

Figure 25: Plot of the difference in Seebeck coefficients against the temperature for several standard thermocouple types[20].

Over the range where the lines are drawn the thermocouple can be used. The range in which the differential thermocouple is used is from 100 °C to 816 °C. The thermocouple type with the most constant difference in Seebeck coefficients over this range is type K. For this reason this type is chosen for the differential thermocouple. The Seebeck coefficient is chosen to have a minimal error. This is the average between the maximum and the minimum Seebeck coefficient in the range resulting in 41±2 µV/°C. The error e_S this can cause in determining the difference is temperature can be expressed as

$$e_S = \frac{\max(S_{Cr} - S_{Al}) - \min(S_{Cr} - S_{Al})}{S_{Cr} - S_{Al}}, \qquad (6.41)$$

where S_{Cr} and S_{Al} are the Seebeck coefficients for respectively the chromel and the alumel electrodes used in a type K thermocouple. This error can be calculated as $e_S = 3$ %.

Both electrode alloys are nickel based, alumel consists of 95 % nickel, 2 % manganese, 2 % aluminum and 1 % silicon and chromel consists of 90 % nickel and 10 % chromium. The fact that the thermocouple is nickel based has some consequences. Firstly nickel is a magnetic material which means that it undergoes

a step change in voltage when the thermocouple reaches its Curie point at 354 °C for type K. Secondly it is a good material to weld to copper because it can form a bond without necessarily melting the copper.

To connect the thermocouple wires to the solid bodies welding is the preferred way since no additional materials need to be added. This prevents the formation of unwanted alloys which may not be vacuum or neutron irradiation compatible or reduce the melting point. For welding a wire to a solid body without distorting the body laser welding is ideal. To form a strong connection the wire should be welded tangentially for a length of several millimeters. A photo of a laser weld of an alumel and a chromel wire to a copper block is shown in *Figure 26*.
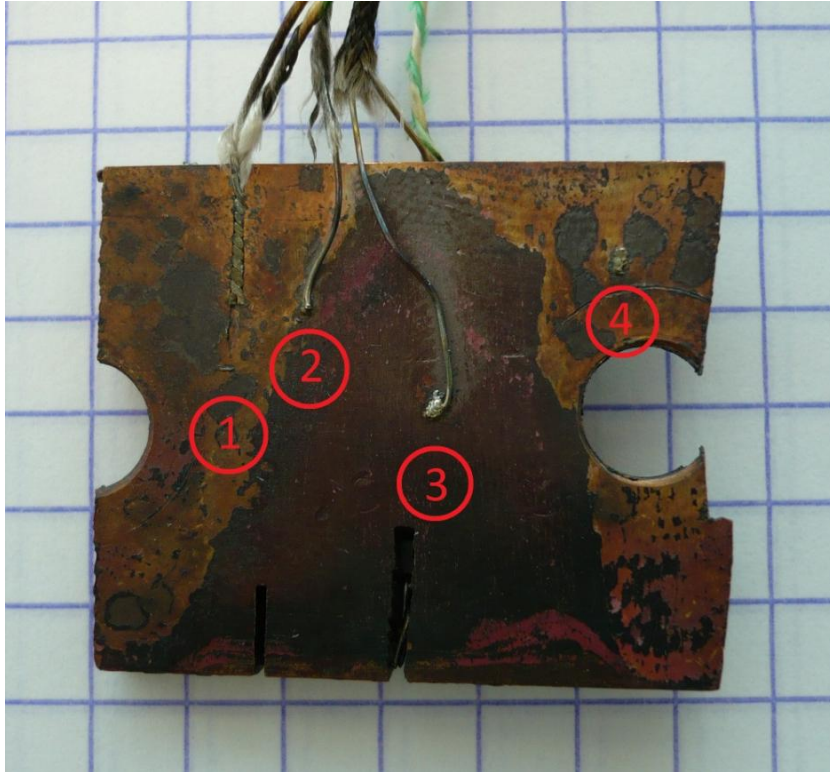

Figure 26: Photo of alumel and chromel wires with a diameter of 0.3 mm laser welded or hammered onto a copper block. The discoloration is caused by the high temperature testing. The background squares have dimensions of 5x5 mm.

The weld indicated by number 2 is an alumel wire laser welded to the copper. Weld number 4 was a chromel wire that was laser welded to the copper but someone pulled the wire too hard. It should be noted that the failure was not in the weld but the wire itself. This means that the weld must have made a stronger bond with the copper. Weld number 3 is a chromel and an alumel wire welded to the copper at the same time, also here one of the wires broke. On the left at number 1 an alumel and a chromel wire are twisted and then hammered into a small groove to act as a reference for the laser welds. The deviations in the different connection types in the range of 22 °C to 720 °C are less than a percent of the total temperature range.

To ensure that the temperature difference between the solid bodies is measured the electrical loop should pass through these bodies. This means that the two thermocouple wires should not be connected directly. If this method is not to produce a parasitic voltage then the joints between the bodies and the thermocouples have to be isothermal. The lumped capacitance method ensures that the temperature variations do not exceed 10 % but this can still produce a large error. Because the cylinder is axisymmetric the temperature is equal at the same height. For a very fast response time the thermocouples can be welded to the upper part of the cylinder but in steady state this will produce an error caused by the fact that the top of the cylinder is hotter than the bottom. The lumped capacitance method assumes the average temperature so in order to measure the average temperature the thermocouples should be welded to half the height. To minimize heat distortion caused by the thermocouples the chromel will be used to connect the two cylinders and this wire will be made as long as possible. Because it is not possible to weld the alumel at the same height at the same side the chromel is put at the far side of the copper cable. This layout is shown in *Figure 27*.
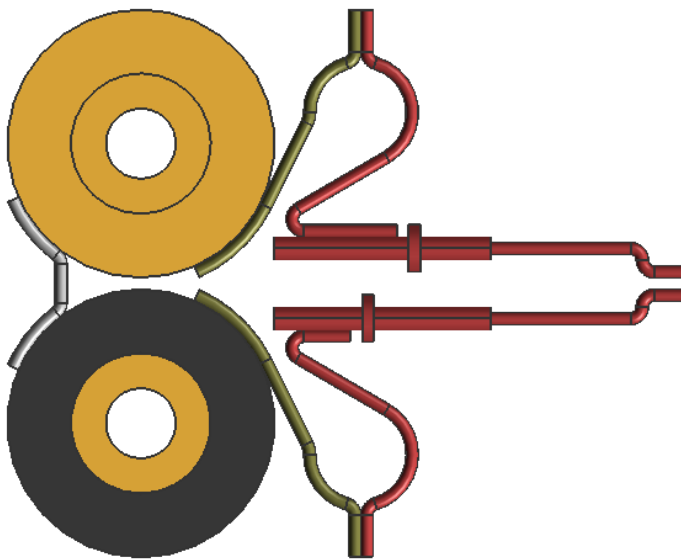

Figure 27: Electrical circuit of the microwave detector. In red is the copper cable connection, in brown is the alumel wire, in grey the chromel wire and in orange the copper cylinders, one of which is coated.

So far everything can be assembled and welded before its installation. The cable however will have to be connected to the alumel wire on the spot. A laser welding machine will be difficult to use because the vacuum vessel will need to be evacuated as the laser may reflect off the vessel walls. Instead a micro-TIG welder will be used. This requires some space to make the weld so the alumel wire and the copper strand from the cable are extended so that they can be bent to a place where they can be welded. The diameter of the differential thermocouple wires is chosen to be the same as the copper strand which is 0.5 mm for the ease of welding.

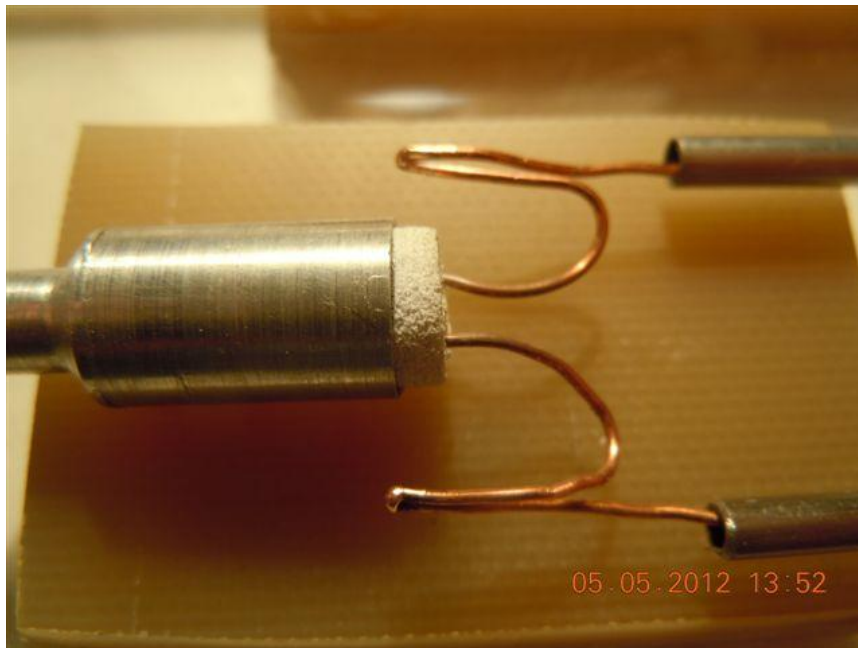A photo of a micro-TIG weld welding two copper strands is shown in *Figure 28*.

Figure 28: Photo of micro-TIG welds performed on copper wires with a diameter of 0.5 mm for the original junction box prototype.

A weld of copper to nickel should be similar to these welds.

Isothermal block

The joints of these two extensions will cause a parasitic signal according to *Chapter 5*. The error e_T this signal causes is the parasitic signal divided by the signal produced to measure the temperature difference as shown in equation (5.5). This gives the following formula for the error

$$e_T = \left| \frac{S_{Cu} - S_{Al}}{S_{Cr} - S_{Al}} \frac{T_3^+ - T_3^-}{T_2 - T_1} \right|, \tag{6.42}$$

where S_{Cu}, S_{Al} and S_{Cr} are the Seebeck coefficients of respectively copper, alumel and chromel. The temperatures correspond to those of *Chapter 5*. The unknown in this equation is the ratio between the difference in junction temperatures and the difference in the solid body temperatures. They can be found by analyzing the heat conduction system through the thermocouples.
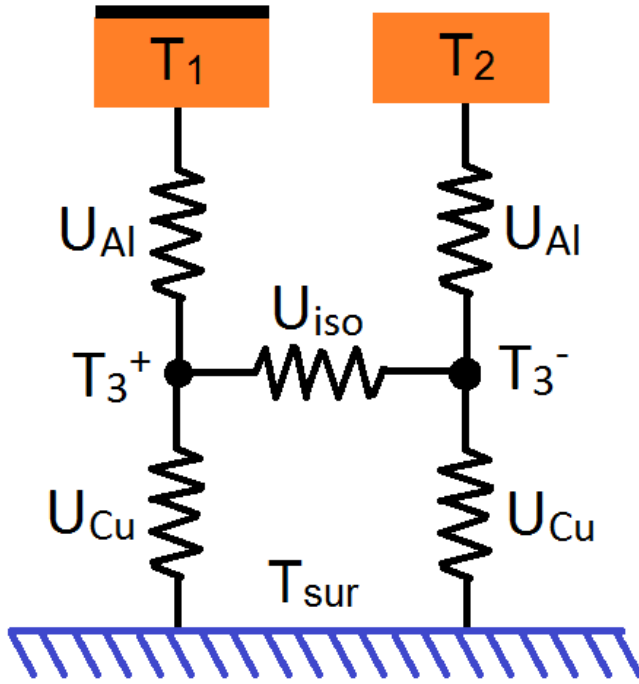
This system is shown in *Figure 29*.

Figure 29: Schematic representation of the thermal conduction system of the electrical circuit. The temperatures T_1 and T_2 of the copper cylinders and the surrounding temperature T_{sur} cause intermediate temperatures at the alumel to copper junctions with temperatures T_3^+ and T_3^-. The isothermal block with overall heat transfer coefficient U_{iso} can equalize these temperatures.

The power balances of the two junctions in presence of an isothermal block are

$$U_{Al}(T_1 - T_3^+) = U_{Cu}(T_3^+ - T_{sur}) + U_{iso}(T_3^+ - T_3^-), \tag{6.43}$$

$$U_{Al}(T_2 - T_3^-) = U_{Cu}(T_3^- - T_{sur}) - U_{iso}(T_3^+ - T_3^-), \tag{6.44}$$

where U_{Al}, U_{Cu} and U_{iso} are the overall heat transfer coefficients of respectively the alumel wire, the copper strands and the isothermal block. Subtracting these two equations yields

$$U_{Al}(T_1 - T_2) = (U_{Cu} - U_{Al} + 2U_{iso})(T_3^+ - T_3^-). \tag{6.45}$$

Rewriting and substituting into equation (6.42) gives

$$\frac{T_3^+ - T_3^-}{T_1 - T_2} = \frac{U_{Al}}{U_{Cu} - U_{Al} + 2U_{iso}}, \tag{6.46}$$

$$e_T = \frac{S_{Cu} - S_{Al}}{S_{Cr} - S_{Al}} \frac{U_{Al}}{U_{Cu} - U_{Al} + 2U_{iso}}. \tag{6.47}$$

Now only the Seebeck coefficients and the overall heat transfer coefficients need to be found. They can be estimated with equation (4.4).

The required parameters are given in *Table 11*.

Table 11: Parameters of the electrical wiring of the microwave detector.

Variable	Symbol	Value
Length of copper strand	L_{Cu}	11 mm
Length of alumel wire	L_{Al}	8 mm
Area of copper strand	A_{Cu}	0.20 mm^2
Area of alumel wire	A_{Al}	0.20 mm^2
Thermal conductivity of copper	k_{Cu}	390 W/mK
Thermal conductivity of alumel	k_{Al}	40 W/mK
Heat transfer coefficient of copper strand	U_{Cu}	7.1 mW/K
Heat transfer coefficient of alumel wire	U_{Al}	1.0 mW/K
Seebeck coefficient of copper	S_{Cu}	2 µV/K
Seebeck coefficient of alumel	S_{Al}	-18 µV/K
Seebeck coefficient of chromel	S_{Cr}	22 µV/K

The isothermal block in the conceptual design is designed to be made out of the ceramic aluminum nitride (AlN). The advantage of this material is that is has a high thermal conductivity k_{iso} and is an electrical insulator. The disadvantage is that it is expensive, brittle and the thermal conductivity degrades under neutron irradiation. Instead of a ceramic copper may be used. It should however be electrically insulated from the thermocouple. This can be done with commercially available ceramic washers. It should also be thermally insulated from the base of the junction box to avoid creating a temperature difference and it should be thermally connected to the ceramic washer. Both can be achieved by using disc springs at the bolts to apply a preload. Both the aluminum nitride and the copper block design are shown in *Figure 30*.
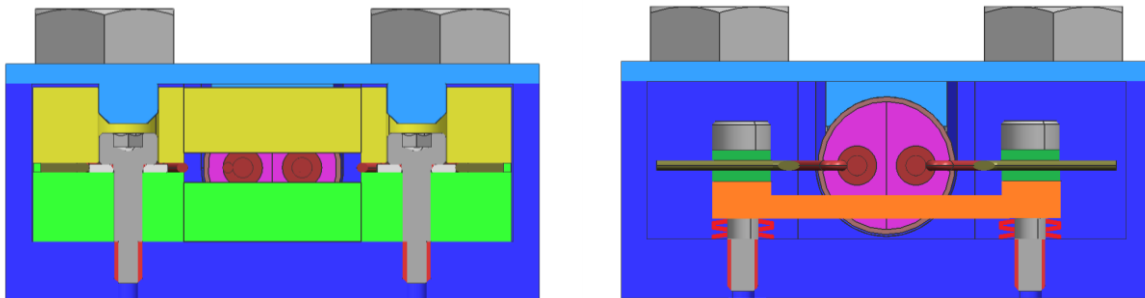

Figure 30: Cross-sections of two different types of isothermal blocks. To the left is the aluminum nitride isothermal block and to the right the copper isothermal block.

The parameters for the isothermal blocks and the errors e_T are given in *Table 12*.

Table 12: Parameters of the isothermal blocks and the error produced by the parasitic signal.

Variable	Symbol	No isothermal block	Aluminum nitride block	Copper block
Length of isothermal block	L_{iso}	-	15 mm^2	15 mm^2
Area of isothermal block	A_{iso}	-	9 mm^2	4 mm^2
Thermal conductivity of isothermal block	k_{iso}	-	180 W/mK	390 W/mK
Heat transfer coefficient of isothermal block	U_{iso}	0 mW/K	108 mW/K	104 mW/K
Error due to parasitic signal	e_T	8.2 %	0.23 %	0.25 %

This table shows that having no isothermal block causes an error of $e_T = 8$ %. When added to the other errors the total error becomes $e_{tot} = 18$ % which is acceptable for measuring high power densities. For the low power density criterion however any slight difference in temperature can produce a parasitic voltage that is higher than the actual voltage produced by the detector. Even in steady state this error is too large producing a total error of $e_{tot} = 24$ %. An aluminum nitride or copper block makes the parasitic signal negligible with errors of only $e_T = 0.2$ %. This will force the two junctions to be isothermal also for low power densities and during transients. For cost effectiveness the copper isothermal block is recommended but the aluminum nitride block can also be used if there turns out to be a problem with the copper block. In the rest of the report the aluminum nitride block is used however because it was developed earlier and a CAD drawing is available for it.

Junction box modifications

The base of the junction box will be welded to the vacuum vessel. This means that both the original junction box and the microwave detector need to use the same base. The design of this base has therefore been conservative and the only modifications are four threaded holes in the bottom for fastening the bolts and enlargement of the design space in the direction of the cable. This is shown in *Figure 31*.
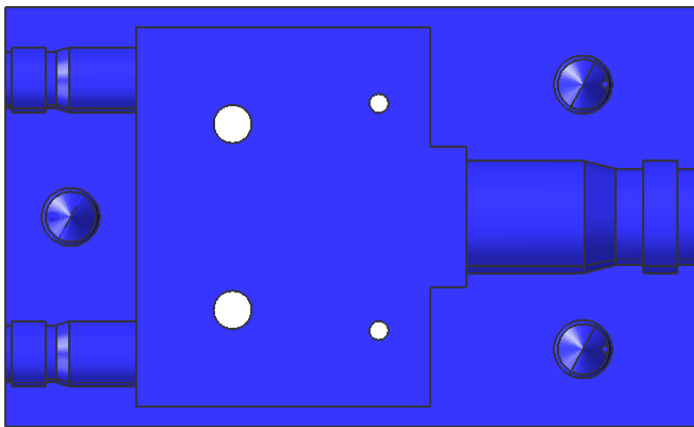

Figure 31: Top view of the modified junction box base. New are the four holes in the base plate and the open area has been enlarged on the right.

Further modifications will include slots or channels in the bottom of the base to allow expansion and contraction of the vacuum vessel without putting too great stresses on the welds to the base. This will reduce the conduction through the bottom of the base and care should be taken that the bolts on the cylinders can provide enough force to increase the thermal contact without failing.

The lid design is not as conservative as the base because it requires large holes to allow microwaves to pass through which is unacceptable for the original junction box. Therefore a different lid will be used on the detector which can be designed freely. An image of the lid (light blue) with the fixation block (yellow) is shown in *Figure 32*.
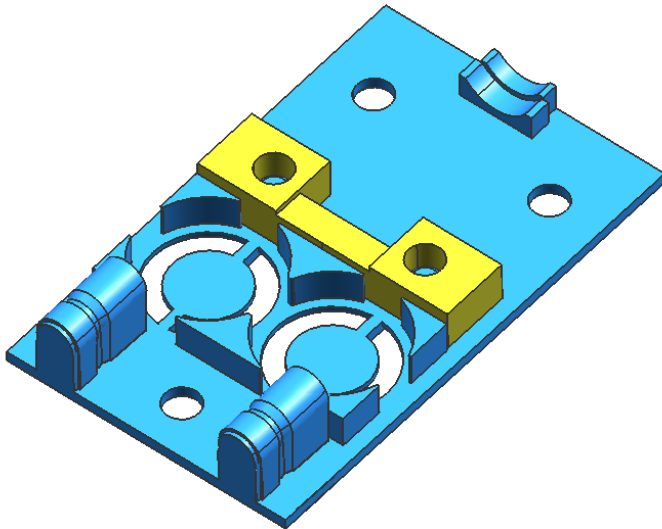

Figure 32: View of the lid of the bottom of the microwave detector (light blue) and the fixation block (yellow). Only the three holes for the bolts and the clamp for the cable are original to the junction box.

The holes for the microwaves are specifically designed to allow the microwaves to reach the reflecting or absorbing surfaces of the cylinders but to keep them away from the interior of the detector and the bolt that fastens the cylinders. Inside the hole a cap is placed to protect the bolt. The cap is connected to the lid by beams that fix it in place and that allow the heat that is generated in the cap to be conducted away. Further protection is made by making sure that the holes have a smaller outer diameter and a larger inner diameter than the cylinders to create an overhang to prevent microwaves from entering directly. The minimum dimension of the hole is then 1.85 mm which is larger than the ECH wavelength of 1.76 mm so microwaves can enter the holes and be absorbed by the cylinders, but the difference is minimal so the actual power that penetrates the holes may be smaller than calculated. Also sharp edges are to be avoided because these can create arcs and may overheat locally. Further protection is made by creating a labyrinth for the microwaves. This is realized by adding pads to the lid that will enclose the cylinders once installed. The spaces that are left between the cylinders and the lid are 0.5 mm. This should be small enough to block the microwaves that are polarized in that direction but the microwaves that are polarized in the other direction may still penetrate to the interior. So the interior should not be considered microwave free. Finally two pins are added onto the lid to position the electrically insulating fixation block on for ease of installation in a difficult position. These will not be necessary if the copper isothermal block is used.

7. Design analysis and experiments

In this chapter first an error analysis is performed and then the design of *Chapter 6* is validated by a microwave detection simulation and a differential thermocouple experiment. The error analysis is crucial in determining which designs meet the maximum error criterion. The microwave detection simulation is performed using the global power balances of the bodies including most predictable steady state non-linear temperature effects. In the simulation the alumina bolt and the aluminum nitride isothermal block are used. Both the maximum and the minimum microwave power are investigated to determine the feasibility of the microwave detector. For the differential thermocouple experiment two copper blocks were connected by a differential thermocouple. Each body was connected with a standard thermocouple for reference. This is used to validate the differential thermocouple and find the error that it produces.

Error analysis

In this design the errors have a crucial role in making the design choices (bolt type and isothermal block). An error analysis is therefore important to determine the total error e_{tot} which can help choose which designs comply with the maximum error e_{max}. An overview of all error sources and expressions for them is given in *Table 13*.

Table 13: Overview of all error sources and their expressions.

Error source	Expression
Radiation	$e_r = \dfrac{\varepsilon \sigma S}{U_{eq}}(T_{max} + T_{sur})(T_{max}^2 + T_{sur}^2)$
Non-constant conduction	$e_U = \dfrac{\left| U_{eq}(T_{max}) - U_{eq}(T_{sur}) \right|}{U_{eq}(T_{sur})}$
Non-constant Seebeck coefficient	$e_S = \dfrac{\max(S_{Cr} - S_{Al}) - \min(S_{Cr} - S_{Al})}{S_{Cr} - S_{Al}}$
Non-zero junction temperature difference	$e_T = \dfrac{S_{Cu} - S_{Al}}{S_{Cr} - S_{Al}} \dfrac{U_{Al}}{U_{Cu} - U_{Al} + 2U_{iso}}$
Non-constant heat capacity	$e_c = \dfrac{|c(T_{max}) - c(T_{sur})|}{c(T_{sur})}$
Non-steady state	$e_t = \exp\left(-\dfrac{U_{eq}}{\rho c V} t_{int}\right)$
Electromagnetic interference	$e_V = \dfrac{U_{eq} \dfrac{dB}{dt} O}{(S_{Cr} - S_{Al})\alpha p S \sqrt{t_{int}/t_s}}$

For both the minimum and maximum microwave power the total error has to be smaller than the maximum error $e_{tot} < e_{max}$ according to the criterion of equation (6.11). The minimum power density is only comprised of the steady state term since the error in the transient term is too high so it is ignored. This causes the non-steady state error of equation (6.15). For the maximum power density both the steady state and transient term must have errors below the maximum error in order to ensure that the error in the microwave power density is also below the maximum error. This results in a total of three error modes that should all fulfill the criterion of equation (6.11).

In general the total error e_{tot} is the sum of all errors e_i when second order effects are ignored

$$e_{tot} = \sum_i e_i. \tag{7.1}$$

Not all error sources contribute to all error modes and some are even of opposite sign so that only the maximum error counts for the total error. This is the case for the maximum power steady state total error

$$e_{tot} = \max(e_r, e_U) + e_S + e_T. \tag{7.2}$$

Infrared heat radiation decreases the temperature for higher temperatures while relaxation of the disc springs will cause an increase in temperature for higher temperatures. While the time relaxation of the disc spring may not be instantaneous like the heat radiation it is impossible for both effects to reinforce each other so the maximum of either source is the worst possible case. The errors from the non-constant Seebeck coefficient e_S and the non-zero junction temperature difference e_T are caused by the conversion of the temperature difference ΔT to a measurable voltage ΔV using the Seebeck effect and are present regardless of the error mode. The maximum power transient total error therefore also has these errors and also the error due to the non-constant heat capacity e_c

$$e_{tot} = e_S + e_T + e_c. \tag{7.3}$$

For the minimum power total error two different error sources become significant. These are the non-steady state error e_t and the electromagnetic interference error e_V

$$e_{tot} = e_S + e_T + e_t + e_V. \tag{7.4}$$

A numerical evaluation of the total errors and a check of the maximum error criterion in all error modes for every design combination can be found in *Appendix E*. In summary only an alumina M3x7 bolt in combination with a copper or aluminum nitride isothermal block satisfy the maximum error criterion.

Microwave detection simulation

In order to simulate the detection of a supplied microwave power first the temperatures of the two solid bodies are simulated. This is done by calculating the temperature every time step by solving the power balances of equations (5.6-5.7). The temperature dependence of the overall heat transfer coefficient is taken into account and this temperature is assumed to be always equal to the temperature of the body. The time dependence of the heat conduction is not taken into account and a minimum integration time of 5 s is necessary to avoid errors caused by time dependent conduction. Now the temperatures can be converted to a voltage via the Seebeck effect and subtracted to yield a voltage difference. The conversion is done by integrating the Seebeck coefficient over the temperature range between the two bodies according to equation (5.1). The electromagnetic noise is then added to this voltage difference and then it is divided by the average Seebeck coefficient to give the temperature difference. This signal contains much noise and it has to be integrated over the integration time to smooth out this noise. The signal is then differentiated and with equation (5.15) the microwave power density is calculated. This procedure is similar to the procedure followed for the microwave detector in the MISTRAL.

First the worst case scenario of the maximum power is analyzed. The first 5.5 s a power density of 3 MW/m² is supplied to simulate startup and then a steady state power density of 1.25 MW/m² is supplied. The surrounding temperature is kept at a constant 100 °C. The integration time is 5 s. The results are shown in *Figure 33*.
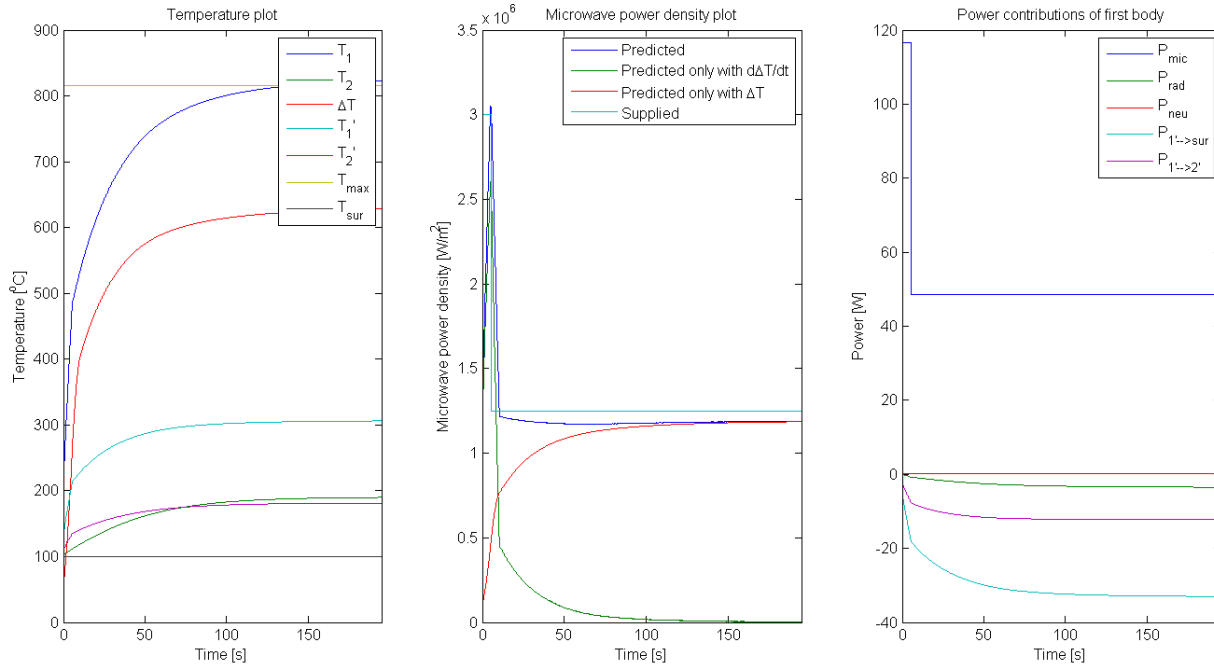

Figure 33: Plots of the temperature (left), microwave power density (middle) and the power contributions of the first body (right) against time. The simulation was performed for the maximum microwave power. Initially the startup power is supplied and further on the maximum steady state power is supplied.

In the plot to the left the temperatures are shown, in the middle plot the microwave power densities are shown and to the right the power contributions of the first (absorbing) body are shown. The temperature plot shows steep initial rises in the temperature due to the startup transient and then the temperatures exponentially decay to the steady state temperatures. For body 1 this is the maximum working temperature which verifies that the conduction design is correct. If this temperature is exceeded slightly this is not a problem since no irreversible damage will occur for at least another hundred degrees but the microwave power density measurement does become unreliable at this point. In the beginning the junction temperature of the second body T_2' exceeds the temperature of the body itself. This means that heat from body 1 is conducted to heat up body 2, but this was expected and does not cause an error. The microwave power density plot shows the supplied and predicted power densities. When the supplied power density stays constant longer than the integration time the deviation from the predicted power density is smaller than 20 %. The plot also shows the contributions of the two terms of equation (5.15) that were used to predict the power density. Finally the power contributions to the first body are given. This shows that the neutron power contribution at maximum microwave power is negligible. Also radiation losses are small compared to the conduction losses resulting in only a small error.

Now the minimum power density of 0.5 kW/m^2 is simulated. This time the integration time is 60 s and a square chirp signal with times ranging from 140 s to 40 s is supplied to analyze the predicted response. The results are shown in *Figure 34*.
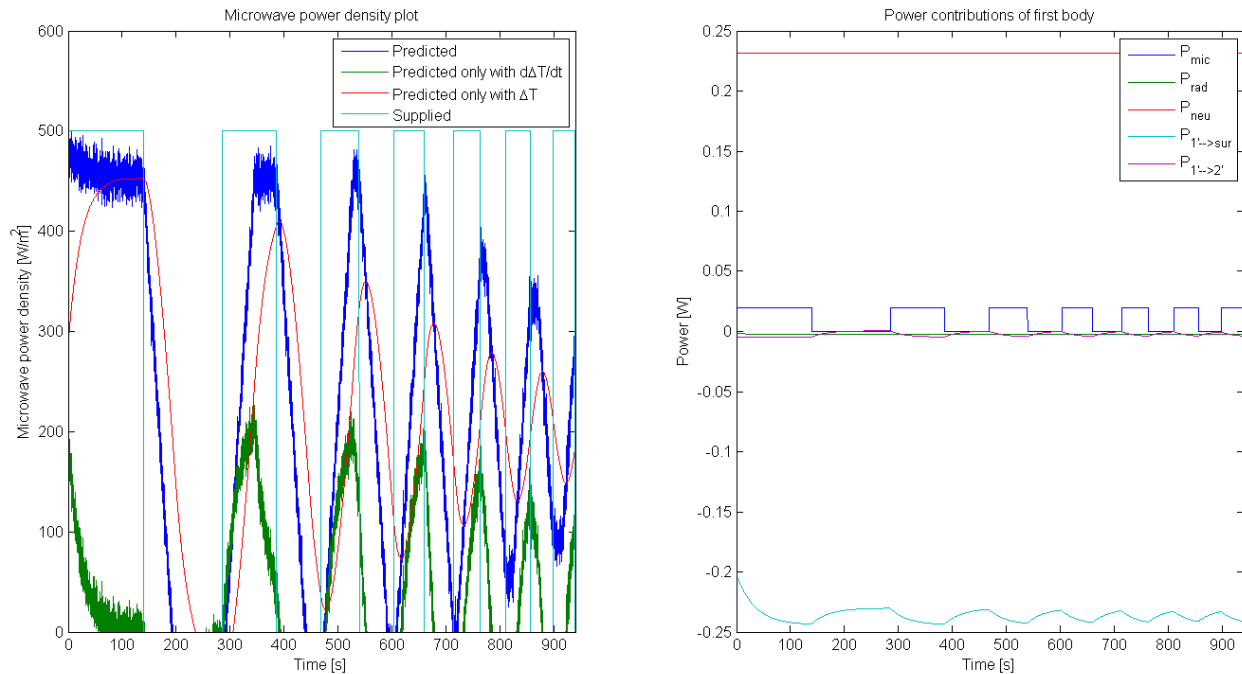

Figure 34: Plots of the microwave power density (left) and the power contributions of the first body (right) against time. The simulation was performed for the minimum microwave power. The minimum microwave power is applied as a square chirp signal.

The microwave power density plot is shown to the left and the power contributions to the first body are shown to the right. The power density plot shows that as long as the supplied power stays constant longer than the integration time (the first four waves) the power density can be determined within the 20 % error range. When the waves become shorter the power density can no longer be accurately determined. The plot of the power contributions shows that the neutron power contribution is much higher than the microwave power, yet this is of no importance since the differential thermocouple cancels out the neutron power. This shows the necessity of using two solid bodies with a differential thermocouple as opposed to a single body with a standard thermocouple as used in low neutron power devices like the Wendelstein-7X stellarator.

Differential thermocouple experiment

The differential thermocouple is a concept that is rarely used since in most cases two standard thermocouples can provide a smaller error in determining a temperature difference because the absolute temperature is known and the Seebeck coefficients does not need to be constant. Therefore it is important that this concept is tested to ensure that the detector will work. Also the fact that the thermocouple wires are not connected directly to each other but via copper bodies is a new concept that needs to be tested.

In this experiment two copper bodies are connected via two differential thermocouples, one that connects the wires directly and one that connects the wires via the copper bodies. Each body also has a standard thermocouple as a reference to the differential thermocouples. The configuration is shown in *Figure 35*.
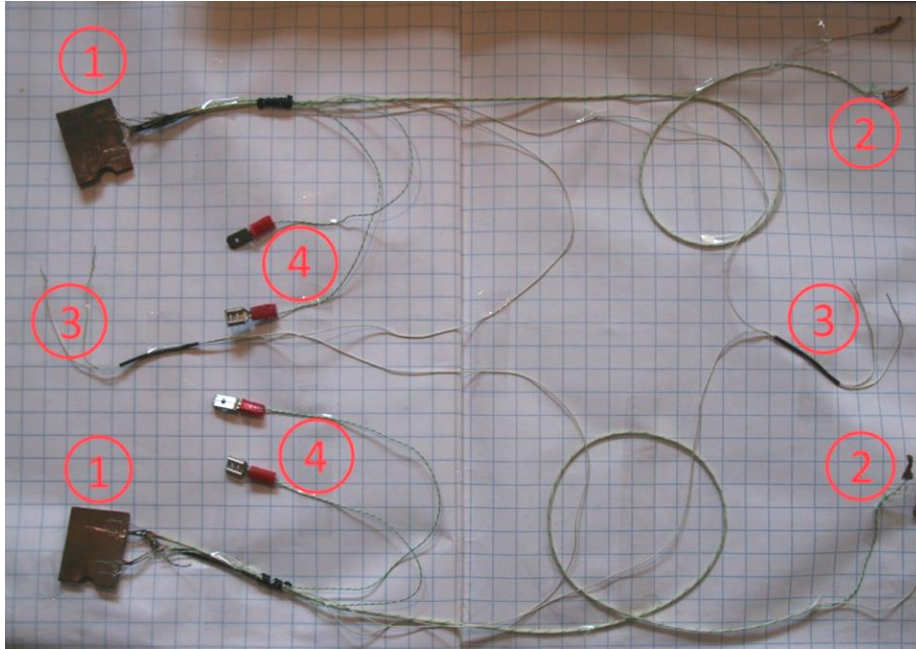

Figure 35: Photo of the layout of the two differential thermocouple and the two reference thermocouples used for the experiment. One of the differential thermocouples has an electric loop through the copper blocks and one is directly connected. All wires have a diameter of 0.3 mm and are hammered into the copper blocks. The background squares have dimensions of 10x10 mm.

The wires are connected to the copper body (1) by twisting the wire and forcing it into a groove. This is a quicker way to connect the wires than by laser welding and *Chapter 6* shows that this has no significant impact on the performance of the thermocouples. The chromel wires connecting the two copper bodies (4) are cut to avoid the possibility of a parallel electrical loop and plugs are fitted on each end to connect the correct wire. The alumel wires (3) are bundled and the voltage differences are measured using voltmeters. The reference thermocouples (2) are also both measured using the same type of voltmeter. All thermocouple wire comes from a single spool of extension cable. This extension cable has not been calibrated but since measuring the exact temperature is not the goal of this experiment this is no problem. The copper bodies are also cut from the same material in order to make sure that no errors can arise from using different materials.

The setup of the experiment is shown in *Figure 36*.

Figure 36: Photo of the experimental setup. The paint dryer and the gas burner are used for temperature control of the copper blocks and three voltmeters are used to record the voltage. The support structures are electrically insulated.

To test the differential thermocouple in a wide range of scenarios a paint dryer is used to heat one copper body and a gas burner is used to heat the other one. Cooling is done by forced or natural convection. A stand and a brick are used to provide a support for the copper bodies. The voltmeters transfer the voltage digitally to a computer using infrared light where the data is stored.

The voltages from the reference thermocouples are then converted to the temperatures T_1 and T_2 using the reference temperature $T_{ref} = 23$ °C which is maintained by the voltmeter. The conversion is non-linear and is evaluated as a polynomial. The assumption has been made that the extension wire has the same characteristics as a real thermocouple type K. The difference between the two reference temperatures $T_1 - T_2$ is then the reference difference in temperature. The voltage measured by the differential thermocouple is divided by the average Seebeck coefficient $S_A - S_B = 41$ µV/°C to yield the predicted temperature difference ΔT. This difference is then subtracted with the reference difference to yield the total error. A distinction can then be made between the error caused by the non-constant Seebeck coefficient and the remaining error.

On the left of *Figure 37* a temperature profile is shown that is analyzed to determine the error caused by the differential thermocouple.
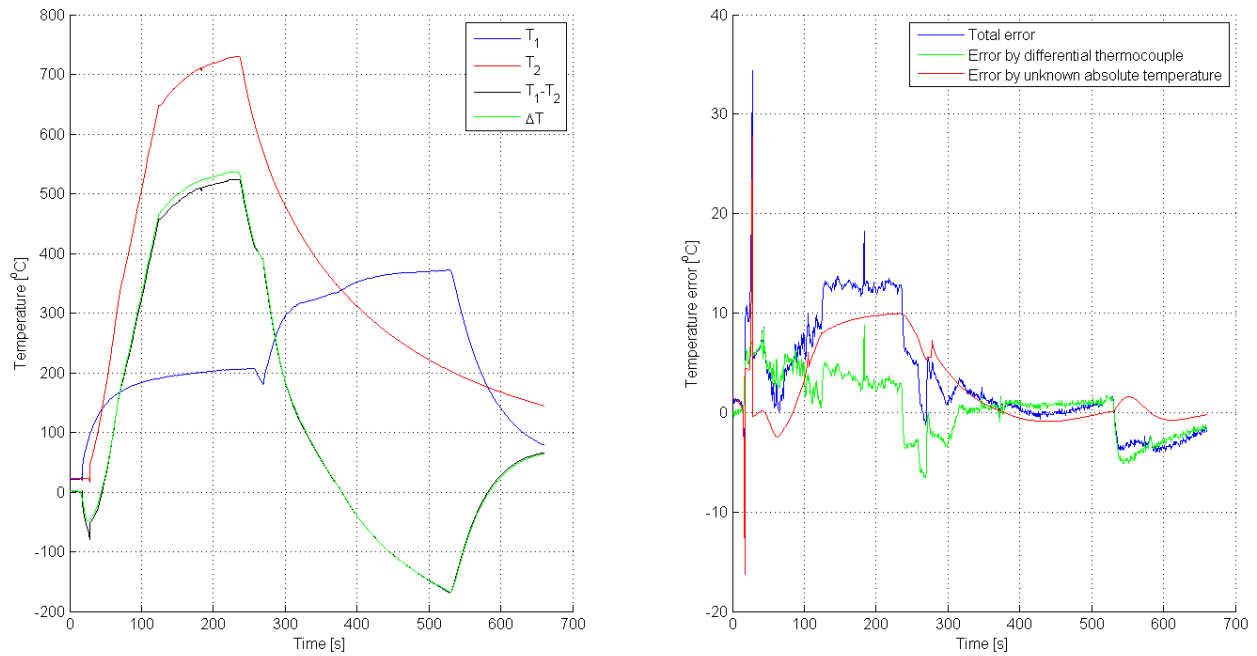

Figure 37: Plots of the temperature (left) and the temperature error (right) against time. In the left plot the black line is the difference in temperatures as measured by the reference thermocouples and the green line is the temperature difference as determined by the differential thermocouple.

Temperature profile T_1 is applied by the paint dryer and T_2 with the gas burner. At around 650 °C the copper started to radiate a lot and for safety the gas burner was turned lower. After 300 seconds it was turned off. The paint dryer has different power settings. Up to around 300 s the power was set to half and then it was set to full power. After 500 s the power was turned off and only the fan was kept on.

These profiles create a varying temperature difference profile that is analyzed to determine the effectiveness of the differential thermocouple. This is shown on the right. The error caused by assuming a constant Seebeck coefficient (in red) is unavoidable and has been analyzed in *Chapter 6*. The remaining error (in green) can be explained by the temperature gradients that are present in the copper due to non-uniform heating and cooling. The directly connected differential thermocouple shows similar behavior which is due to the fact that the reference thermocouples are placed at different positions than the differential thermocouple. The solid bodies of the microwave detector are designed to minimize this error by axisymmetry and placing the thermocouples at the same height. This experiment proves that the theory discussed in *Chapter 5* is valid and can be applied in the microwave detector.

8. Manufacturing, assembly and calibration

Apart from the functionality of the detector other important considerations in the design are manufacturability, assembly and calibration of the detector. First the manufacturing techniques of all custom components are discussed. Then the pre-assembly in a workshop and the final assembly in the vacuum vessel are discussed. Then it is shown how a single detector is used to determine the amount of torque the bolts in the detector require and finally a method for collectively calibrating all detectors after installation in the vacuum vessel is given.

Manufacturing

Manufacturing of the junction box bases and the lids can be done similar to the prototype shown in *Appendix B* or they can be manufactured by 3D printing techniques if the properties of the stainless steel still suffice. The copper cylinders are axisymmetrical and can simply be made by turning. In case the copper isothermal block is chosen for the design it can be manufactured by milling. If the aluminum nitride isothermal blocks are used then they can also be manufactured by milling but then they also need to be fired to harden them and take their final shape. The ceramic coating, which is a mix of alumina and titania, of one of the copper cylinders can be applied in the same manner as used in the tests at the MISTRAL[11]. There it was also applied on top of copper. The method of application is however unknown. Finally one more part that is not commercially available is the specially designed disc spring used to control the conduction. These disc springs are made out of a super-alloy called A286 and the precise dimensions of the disc springs are of importance so these will need to be custom made. All other parts are commercially available.

Assembly

Assembly of the detector should preferably be done in a workshop rather than in the vacuum vessel. This was an important design consideration. An important step is therefore to decide before installation which junction boxes will be used as microwave detectors. This way they can be installed as microwave detectors and later when necessary they may be converted to accommodate the original junction box. All parts can now be pre-assembled in a workshop leaving only micro-TIG welding of the cable to the differential thermocouple, the welding of the junction box base to the vacuum vessel and placing the lid on the base to be done in-vessel. In case the aluminum nitride isothermal block is used the top fixation part may be placed either on the two pins on the lid or already in the junction box depending on the angle under which the detector is located.

The pre-assembly should start with the electrical circuit of the differential thermocouple. The thermocouple wire should be cut to size and laser welded to the copper cylinders. Then the conduction system can be installed. The two bolts with the disc springs, washers and copper cylinders can be screwed loosely into the junction box base. Then they should be carefully and torque controlled screwed tighter until the desired torque is reached. How large this torque should be is explained further on. After both bolts are tightened they should be fixed into place by either the inorganic adhesive Thermoguss 2000 or by a small tack/laser weld placed at the bottom of the bolts. Now all that is remaining is the installation of the isothermal block. This should be a straightforward operation as the amount of torque has no direct impact on the performance of the detector.

Calibration

Finally there is the step of calibration of the detector. In order to find out what the amount of torque is that should be applied to the bolts a prototype identical to the detectors that will actually be installed in ITER should be made. It should be assembled in a similar way and with the same boundary conditions as will be present in ITER except for the fixation of the bolts. This includes a large stainless steel block simulating the vacuum vessel wall which acts as the heat sink of the detector. In *Figure 38* a CAD model of the original junction box is shown including the welds of the junction box to the vacuum vessel.
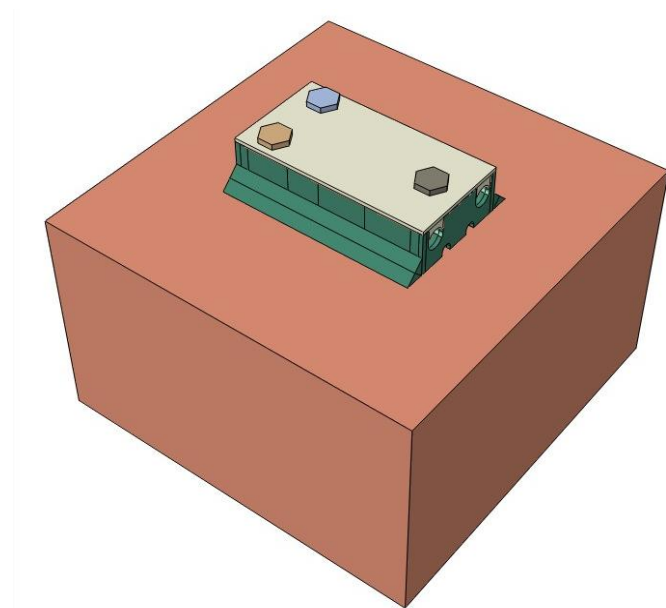

Figure 38: CAD model of the original junction box welded onto the vacuum vessel[21].

This setup should be placed in the MISTRAL facility where it should be subjected to a microwave power. An analysis similar to that of the solid body bolometer used for Wendelstein-7X should be performed on the cool down phase to determine the equivalent overall heat transfer coefficient of equation (5.15). This can be done as a function of the amount of torque that is applied to both bolts. Ideally this heat transfer coefficient should be as low as possible but high enough so that the solid bodies do not overheat under the maximum steady state microwave power. This ideal value can be found experimentally. A margin should be ensured for this heat transfer coefficient since an error in applying the torque may occur.

After the assembly of the detectors in the vacuum vessel a collective calibration of all detectors is possible. By sending stray microwave power through the vessel the detectors will start to heat up. When the microwave power is then switched off the detectors will start to cool down and this curve can be analyzed again to determine the individual equivalent heat transfer coefficients of all detectors. This way any detector that was broken during installation can also be traced and repaired or removed.

9. Discussion and conclusion

To conclude this report a conclusion of the proposed design is presented followed by a discussion on the design and several recommendations including possibilities for further work.

Conclusion

The only measurement option that is considered to be capable of meeting the requirements was found to be solid body bolometry. Two identical metal bodies, one with a microwave absorbing coating and one bare, are connected in series with a so called differential thermocouple. First it was proven that the voltage over this differential thermocouple is a measure for the temperature difference between the two bodies using the Seebeck effect. Secondly a relation has been deducted from the global power balance difference of the bodies between the microwave power density and the temperature difference. This relation shows that heat radiation cannot be used to cool the detector since it cannot be resolved with the temperature difference alone. For heat conduction this is possible independent of the surrounding temperature as long as the conduction system is symmetric.

The solid bodies are be made out of copper for its good thermal conductivity and relatively high melting point. The shape will be cylindrical to assure a uniform temperature at every height and for ease of manufacturing. The fact that the lumped capacitance method can be invalid during the startup phase therefore requires that the thermocouple wires are connected to the cylinder at a single height. The ratio of volume over exposed surface is practically defined by the height of the junction box. This fixes the thermal response time of the copper cylinders. The response time of the measurement however can be faster at the expense of accuracy if the thermocouples are connected closer to the exposed surface of the cylinders. The ratio is actually too large to reach the maximum achievable transient sensitivity since a microwave absorption coefficient larger than unity would be required. Because this is impossible an absorbing ceramic coating is applied that has the highest known absorption coefficient.

The amount of conduction that is required is tuned such that for the maximum steady state microwave power the maximum temperature in the bodies is not exceeded, this determines the maximum steady state sensitivity. The conduction has to be temperature independent to resolve the microwave power. This is achieved by fastening the copper cylinders with a bolt and a disc spring on the junction box base separated by a ceramic washer. The maximum temperature of the bodies is limited by the modulus of elasticity of the disc spring which plummets beyond this temperature. For this reason the disc springs are made out of a high temperature precipitation hardening iron base super-alloy A286. Two types of bolts have been investigated, namely an alumina M3x7 bolt and a stainless steel M2x8 bolt with a ceramic cover. The tensile strength of the alumina bolt was found to be too low, but a copper foil between the ceramic washer and the junction box base should reduce the required tensile strength to below a safe level. When the temperature dependence of the conduction was analyzed for both bolts it was found that only the alumina bolt remains constant enough in temperature to meet the requirements.

The differential thermocouple type that is chosen is type K, mainly for its linear behavior. This type consists of alumel and chromel wires, both containing at least 90 % nickel. At some point the leads of this differential thermocouple need to be connected to a copper cable. A temperature difference between these connections can produce a parasitic signal. This produces a significant error in determining the

microwave power in steady state. In a transient case this error can be much higher. Therefore an isothermal block is recommended. Both a copper and an aluminum nitride block have been proposed, both of which will reduce this error to below a percent. For cost effectiveness the copper block is recommended.

The design has been concluded now, only a validation of the design and several practicalities such as manufacturing, assembly and calibration remain. Validation has been done with a microwave detection simulation containing most non-linear temperature effects and an experiment involving a differential thermocouple. The results for both tests complied with the expectations thereby validating these aspects of the design. The manufacturing of the microwave detector housing is mostly analogous to the original junction box. The added custom parts are the copper cylinders, the isothermal block and the disc springs. All other parts are commercially available. Assembly can mostly be done in a workshop and only a few basic operations have to be performed inside the vacuum vessel. After assembly a collective calibration of all detectors is possible by simply heating the detectors and analyzing the cool down phase.

Finally an assessment is made whether the goals of the detector have been accomplished. The primary goal was the protection of in-vessel components from overheating. This imposed several requirements on the detector, all of which have been met, and thereby this goal has been achieved. The secondary goal was protection of the sensitive diagnostics. This requires response times in the order of several milliseconds. In the current design the response time is more in the order of a second. This can be improved, but this will be at the cost of accuracy which can then no longer meet the requirements set by the primary goal. Finally an effort was made to use the detector as a diagnostic device for which a minimum microwave power density was defined. This required a very sensitive detector but with a combination of proper cooling and a high maximum temperature this can be achieved. An overview of the specification of the detector is given in *Appendix D*.

Discussion and recommendations

A first recommendation for further work would be to investigate the absorbing ceramic coating used in Wendelstein-7X for the ECH frequency of 170 GHz and the CTS frequency of 60 GHz. Different ceramic coatings may be investigated as well to find optimum absorption coefficients for these frequencies. Preferably the ratio between the absorption coefficients of these frequencies should equal the ratio for the systems it is designed to protect.

Secondly a finite element standing wave analysis may be performed on the detector to find the actual absorbed microwave power as a function of the microwave power density before it impinges on the detector. This may lead to the conclusion that the dimensions of the holes in the lid are too small for the desired transient sensitivity and need to be enlarged. This will be at the cost of microwave protection of the interior of the detector, but since no microwave sensitive parts are present there this may be acceptable. This can be optimized using the same finite element method. Another way to increase the transient sensitivity is to reduce the volume of the copper bodies since thermal inertia is not a critical criterion yet. Care should be taken however that this will also increase the already critical Biot number.

The steady state sensitivity is already critical as it is fixed by the maximum steady state power. This steady state power is still under debate however and maximum power densities as low as 250 kW/m^2 have been

mentioned. This should have no significant consequences for the design as the bolt can simply be loosened or the copper foil removed thereby reducing the force that controls the conduction. Another way to circumvent this critical steady state power is by placing a slot in the junction box base between the two copper cylinders. This will reduce heat conduction from body to body thereby decreasing the temperature in the reflecting body. This will in turn increase the temperature difference and thus the steady state sensitivity. This slot will also help reduce strain in the welds of the junction box by expanding and contracting together with the vacuum vessel.

For fastening the copper cylinders on the junction box base the aluminum nitride M3x7 bolt was preferred above the stainless steel M2x8 bolt because the force provided by the stainless steel bolt decreases with temperature. The reason for this was that the thermal expansion of the bolt was too large. The advantages of metal above ceramic are clear however. They are less brittle and have a higher tensile strength, which is necessary since the diameter of the bolt is smaller to allow for a ceramic cover for electrical insulation. Ideally a metal bolt would be used that has a low thermal expansion coefficient. A metal with a very low expansion coefficient is molybdenum, possibly alloyed for increased tensile strength and processability. It might however be difficult to weld it to the junction box base since the melting temperature of molybdenum is as high as 2623 °C. An in-between choice might be titanium. It has very good mechanical properties and a reasonably low melting temperature of 1668 °C. Another option may be to use expansive washers possibly made out of manganese instead of stainless steel washers. Mechanical properties are not so important here and the melting point of manganese is 1246 °C which is well above the maximum working temperature of the disc springs.

Regardless of whether a ceramic or a metal bolt is chosen a finite element thermal analysis and a prototype should be made to validate the conduction design both numerically as well as experimentally. Experiments can provide input for the thermal analysis so that ultimately both should predict similar results. Then the thermal analysis can be used to simulate the most extreme conditions to evaluate the performance of the detector over the entire work range.

When a higher response time is desired there is the possibility of connecting the thermocouple wires closer to the exposed surface. The response time is quadratic with the distance from the exposed surface to the thermocouple, as shown in equation (6.2), which allows for a drastic decrease in the response time. This will however be at the risk of reduced accuracy due to the non-uniformity of the temperature distribution in the solid body because the Biot number during transients can be above the critical level.

Finally it is recommended that the signal produced by the differential thermocouple is processed parallel to optimize the integration time for every scenario that is of interest. For example for protection of the semiconductors a maximum microwave power that is allowed may be defined which if exceeded should trigger an alarm. This will require only a very short integration period since the detector will quickly heat up and a false alarm is unlikely. In the other extreme however the microwave power may barely exceed the minimum, for a very short integration time only noise will be measured. So in parallel to the protection system a monitoring system may be installed with a long integration time that analyzes how the microwave power behaves in the vessel. In between these extreme cases several more integration periods may be defined which can all be processed in parallel.

10. References

[1]   M. Clough, F. Gandini. *Interface Control Document (ICD) between Electron Cyclotron Heating and Current Drive (PBS 52) - Diagnostics (PBS 55)* 2013.

[2]   Johan W. Oosterbeek, Victor S. Udintsev, George Vayakis, Antoine Sirinelli, Matthias Hirsch, Heinrich P. Laqua, Franco Gandini, Nick Maassen, Yunxing Ma, Matthew Clough, Mike J. Walsh, Christopher Watts. *Loads due to Stray Microwave Radiation in ITER* 2014.

[3]   G. Vayakis. *The ITER radiation environment for diagnostics.*

[4]   Vayakis G. *55.A0 Magnetic Diagnostic System Design Description Document* 2014.

[5]   Pedro A. Molina Cabrera. *Pyroelectric Detectors for ECRH Stray Radiation in the W7-X Stellarator; A short feasibility study* 2013.

[6]   Stefan Paquay. *Improved Measurement of Microwave Stray Radiation* 2012.

[7]   Hugo van den Brand. *Fluid Bolometer measurements on the MISTRAL* 2011.

[8]   Johan W. Oosterbeek. *Bachelor project on monitor for microwave stray radiation power* 2014.

[9]   Wikipedia: *Thermoelectric effect*. http://en.wikipedia.org/wiki/Thermoelectric_effect.

[10]   Frank P. Incropera, David P. Dewitt, Theodore L. Bergman, Adrienne S. Lavine. *Foundations of Heat Transfer.*

[11]   M. Hirsch, H. P. Laqu, D. Hathiramani, J. Oosterbeek, J. Baldzuhn, C. Biedermann, H. v d Brand, A. Cardella, V. Erckmann, R. Jimenez, R. König, M. Köppen, S. Parquay, D. Zhang and the W7-X Team. *The Impact of Microwave Stray Radiation to In-Vessel Diagnostic Components.*

[12]   M. Hirsch, S. Mettchen, D. Hathiramani, H. Laqua. *Dokumentation des Referenz Bolometers* 2011.

[13]   Wikipedia: *Seebeck coefficient*. http://en.wikipedia.org/wiki/Seebeck_coefficient.

[14]   Yunxing Ma (IO), Matthias Hirsh (IPP), Johan Oosterbeek (Tu/e). *R&D Report: Electron Cyclotron Wave Irradiation Test on ITER High-Frequency Magnetic Sensor (PBS 55.AJ) in the MISTRAL Facility*

[15]   High temp metals: *A-286 Technical data*. http://www.hightempmetals.com/techdata/hitempA286data.php.

[16]   Wikipedia: *Standard deviation*. http://en.wikipedia.org/wiki/Standard_deviation.

[17]   Ma Y. *PBS 55.AJ Report: Thermal Conductance Assessment for ITER High-Frequency Magnetic Sensor* 2014,

[18]   Harold Patscheider GmbH: *Thermoguss 2000*. http://patscheider.de/en/thermoguss-2000.html

[19]   Engineer's edge: *Springs Washer Belleville Equation*. http://www.engineersedge.com/belleville_spring.htm.

[20]   Omega: *Reference temperaturs*. http://www.omega.com/temperature/z/pdf/z021-032.pdf.

[21]   L.T. Calcoli. *Junction Box analysis* 2013.

Appendix A: Minimum isotropic stray radiation

A rough estimation of the expected power load can be obtained from a global power balance of the microwave stray radiation background. The fraction of total input power P that is absorbed before it is converted to isotropic stray radiation is α_s, so the total stray radiation power is $P(1 - \alpha_s)$. This power is eventually absorbed by either the plasma, the first wall or through apertures in the wall. The stray radiation power is assumed to be uniform in the vessel so that one microwave power density p can be used everywhere. The powers that are absorbed by the plasma, the first wall (blankets and divertor) and the apertures are then respectively $p\alpha_p A_p$, $p\alpha_{Be} A_{Be}$, $p\alpha_W A_W$ and pA_a, where A is the area. Equating this to the total input power and rewriting gives the present power density p[11]

$$p = \frac{P(1 - \alpha_s)}{\alpha_p A_p + \alpha_{Be} A_{Be} + \alpha_W A_W + A_a}.$$
(A.1)

The variables that are used are given in *Table 14*.

Table 14: Parameters of the ITER vacuum vessel and ECH system.

Variable	Symbol	Value
Total ECH power	P	20 MW
First pass plasma absorption	α_s	0.99
Isotropic plasma absorption	α_p	0.10
Beryllium absorption	α_{Be}	0.008
Tungsten absorption	α_W	0.010
Plasma surface	A_p	680 m^2
Beryllium first wall surface	A_{Be}	708 m^2
Tungsten first wall surface	A_W	150 m^2
Aperture area	A_a	44 m^2

This yields a microwave power density in the vessel of $p = 1.7$ kW/m^2.

However behind the blankets the power density may be lower than this. To find out what the ratio of power density between the plasma and the first wall and behind the blankets is ray tracing is used. This simple approximation of the Maxwell equations is possible because the largest dimension (10 mm) is larger than the wavelength of the microwaves (1.76 mm). The blankets are assumed to be blocks with dimensions L x W x H spaced by a gap D between the blankets and spaced from the flat vacuum vessel by a gap B. The angle of incidence for a ray is θ.

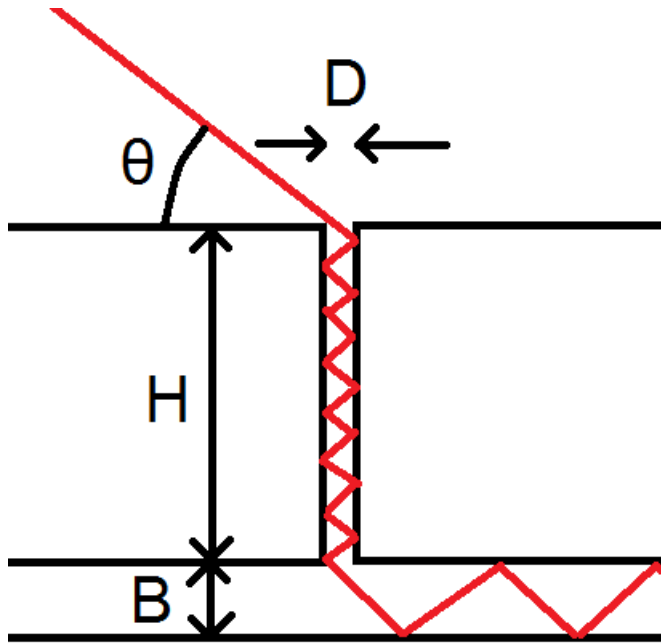An example of a ray is shown in *Figure 39*.

Figure 39: Schematic representation of the gaps between the blankets and the vacuum vessel acting as a channel for microwave rays. The dimensions given are characteristic for the microwave power density behind the blankets.

All material on which the rays reflect behind the blankets is assumed to be stainless steel with an absorption coefficient α_{SS}. The amount of reflections for a ray with an incidence angle θ until it reaches the bottom of the blanket is

$$n_z(\theta, z) = \frac{z}{D \tan(\theta)}.$$
(A.2)

The power ratio at this point is then

$$i_z(\theta, z) = (1 - \alpha_{SS})^{n_z(\theta, z)}.$$
(A.3)

At the bottom of the blanket the rays may get trapped behind the blanket and the vacuum vessel, or be reflected back towards the plasma. The critical angle for which all rays are trapped is

$$\theta_c = \arctan\left(\frac{B}{2D}\right).$$
(A.4)

The power ratio at the entrance of the gap between the blanket and the vacuum vessel is then exactly a half because there is an equal chance for the ray to enter the left or the right gap

$$i_c(\theta < \theta_c) = \frac{1}{2}.$$
(A.5)

For an angle larger than the critical angle this depends on the place where the ray leaves the bottom of the blanket. The power density at this point is assumed uniform so that the power ratio becomes

$$i_c(\theta > \theta_c) = \frac{B}{4D \tan(\theta)}. \tag{A.6}$$

Finally the ray will lose some intensity as it travels between the blanket and the vacuum vessel. The amount of reflections up to that point in x-direction are

$$n_x(\theta, x) = \frac{x \tan(\theta)}{B}, \tag{A.7}$$

and a power ratio in this direction of

$$i_x(\theta, x) = (1 - \alpha_{SS})^{n_x(\theta, x)}. \tag{A.8}$$

In y-direction this has the same form

$$n_y(\theta, y) = \frac{y \tan(\theta)}{B}, \tag{A.9}$$

$$i_y(\theta, y) = (1 - \alpha_{SS})^{n_y(\theta, y)}. \tag{A.10}$$

At any point under the blankets rays may come from all four edges of the blanket. Two from each side of the x-direction and two from the y-direction. The total power ratio per angle of incidence is then

$$i(\theta < \theta_c) = i_z(\theta)i_c(\theta < \theta_c)\big[i_x(\theta, x) + i_x(\theta, L - x) + i_y(\theta, y) + i_y(\theta, W - y)\big], \tag{A.11}$$

$$i(\theta > \theta_c) = i_z(\theta)i_c(\theta > \theta_c)\big[i_x(\theta, x) + i_x(\theta, L - x) + i_y(\theta, y) + i_y(\theta, W - y)\big]. \tag{A.12}$$

Averaging these power ratios gives the power ratio for isotropic radiation. A radiation map for isotropic radiation is shown in *Figure 40*. The variables used to calculate this are given in *Table 15*.

Table 15: Parameters of the blankets and the gaps between the blankets and the vacuum vessel.

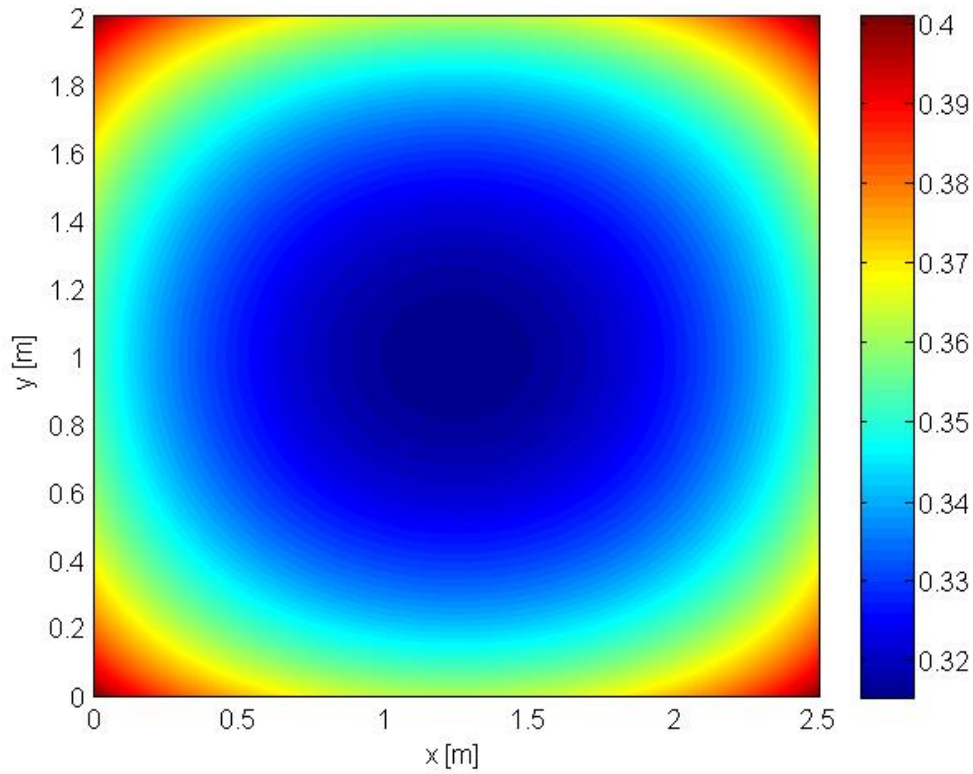| Variable	Symbol	Value
Stainless steel absorption	α_{SS}	0.01
Blanket length	L	2.5 m
Blanket width	W	2.0 m
Blanket height	H	50 cm
Gap width blanket-vacuum vessel	B	20 mm
Gap width blanket-blanket	D	10 mm

Figure 40: Map of the microwave power behind the blankets as a ratio of the microwave power in the vessel for isotropic stray radiation. In the corners the maximum microwave power is present and in the center the minimum.

The center of the blanket has the lowest power ratio. So to calculate the minimum power ratio this point is analyzed further

$$i(\theta < \theta_c) = i_z(\theta)i_c(\theta < \theta_c)\big[2i_x(\theta, L/2) + 2i_y(\theta, W/2)\big], \tag{A.13}$$

$$i(\theta > \theta_c) = i_z(\theta)i_c(\theta > \theta_c)\big[2i_x(\theta, L/2) + 2i_y(\theta, W/2)\big]. \tag{A.14}$$

The power ratio i as a function of the angle of incidence θ is shown in *Figure 41*.
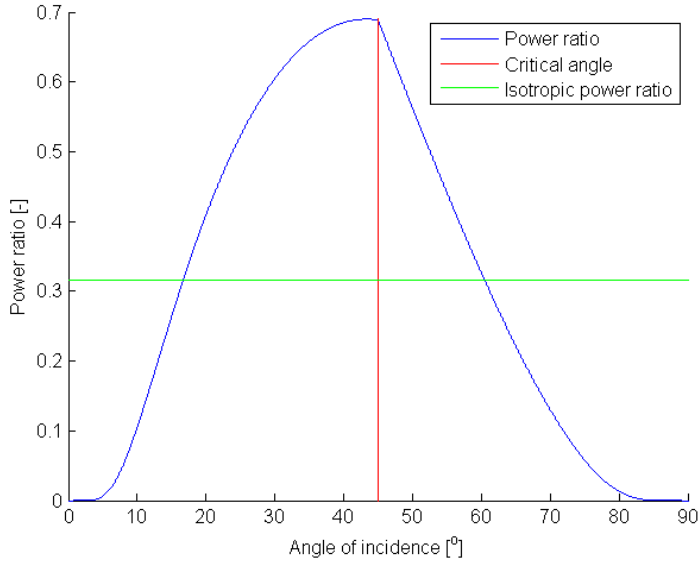

Figure 41: Plot of the power ratio at the center behind the blanket as a function of the angle of incidence.

This figure shows that at an angle of incidence of 45° the power ratio is the highest, almost 0.7. This means that a directed beam wider than one blanket from this angle has only a 30 % reduction in power density. To obtain the power ratio for isotropic radiation however equations (A.13-A.14) are integrated over all angles

$$\bar{\iota} = \frac{4}{\pi}\int_0^{\theta_c} i_z(\theta,H)i_c(\theta < \theta_c)i_x(\theta,L/2)d\theta + \frac{4}{\pi}\int_{\theta_c}^{\frac{\pi}{2}} i_z(\theta,H)i_c(\theta > \theta_c)i_x(\theta,L/2)d\theta$$
$$+\frac{4}{\pi}\int_0^{\theta_c} i_z(\theta,H)i_c(\theta < \theta_c)i_y(\theta,W/2)d\theta + \frac{4}{\pi}\int_{\theta_c}^{\frac{\pi}{2}} i_z(\theta,H)i_c(\theta > \theta_c)i_y(\theta,W/2)d\theta, \tag{A.15}$$

$$\bar{\iota} = \frac{2}{\pi}\int_0^{\theta_c} (1-\alpha_{SS})^{n_z(\theta,H)+n_x(\theta,L/2)}d\theta + \frac{B}{\pi D}\int_{\theta_c}^{\frac{\pi}{2}} (1-\alpha_{SS})^{n_z(\theta,H)+n_x(\theta,L/2)}\frac{d\theta}{\tan(\theta)}$$
$$+\frac{2}{\pi}\int_0^{\theta_c} (1-\alpha_{SS})^{n_z(\theta,H)+n_y(\theta,W/2)}d\theta + \frac{B}{\pi D}\int_{\theta_c}^{\frac{\pi}{2}} (1-\alpha_{SS})^{n_z(\theta,H)+n_y(\theta,W/2)}\frac{d\theta}{\tan(\theta)}, \tag{A.16}$$

$$\bar{\iota} = \frac{2}{\pi}\int_0^{\theta_c} (1-\alpha_{SS})^{\frac{H}{D\tan(\theta)}+\frac{L\tan(\theta)}{2B}}d\theta + \frac{B}{\pi D}\int_{\theta_c}^{\frac{\pi}{2}} (1-\alpha_{SS})^{\frac{H}{D\tan(\theta)}+\frac{L\tan(\theta)}{2B}}\frac{d\theta}{\tan(\theta)}$$
$$+\frac{2}{\pi}\int_0^{\theta_c} (1-\alpha_{SS})^{\frac{H}{D\tan(\theta)}+\frac{W\tan(\theta)}{2B}}d\theta + \frac{B}{\pi D}\int_{\theta_c}^{\frac{\pi}{2}} (1-\alpha_{SS})^{\frac{H}{D\tan(\theta)}+\frac{W\tan(\theta)}{2B}}\frac{d\theta}{\tan(\theta)}. \tag{A.17}$$

Calculating this equation gives an isotropic power ratio of $\bar{\iota} = 0.316$. Combining this with the previously found power density of $p = 1.7$ kW/m² the minimum power density behind the blanket becomes $p_{min} = 0.5$ kW/m².

Appendix B: Junction box images

The slight differences between the CAD drawing of the junction box (*Figure 42*) and the technical drawing and the prototype (*Figures 38-39*) are caused by the fact that this junction box has been modified after the prototype was made.
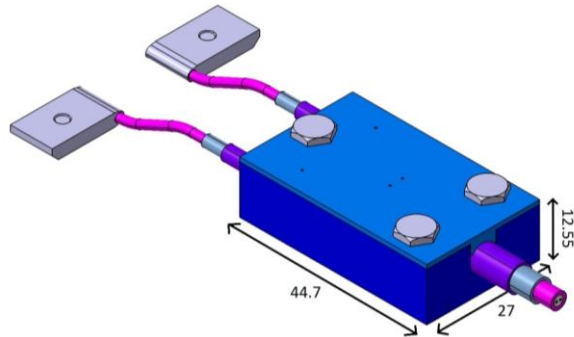

Figure 42: The original junction box in which the detector will be placed. The dimensions are in millimeters.
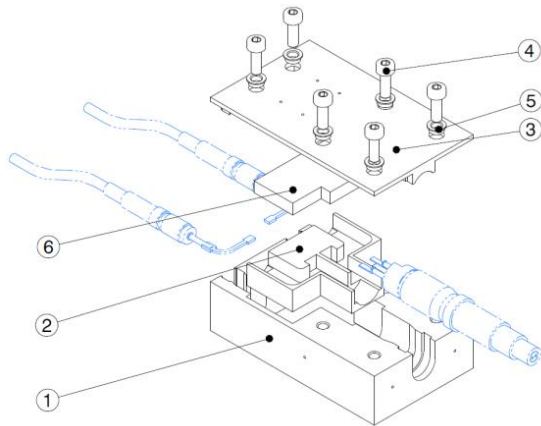

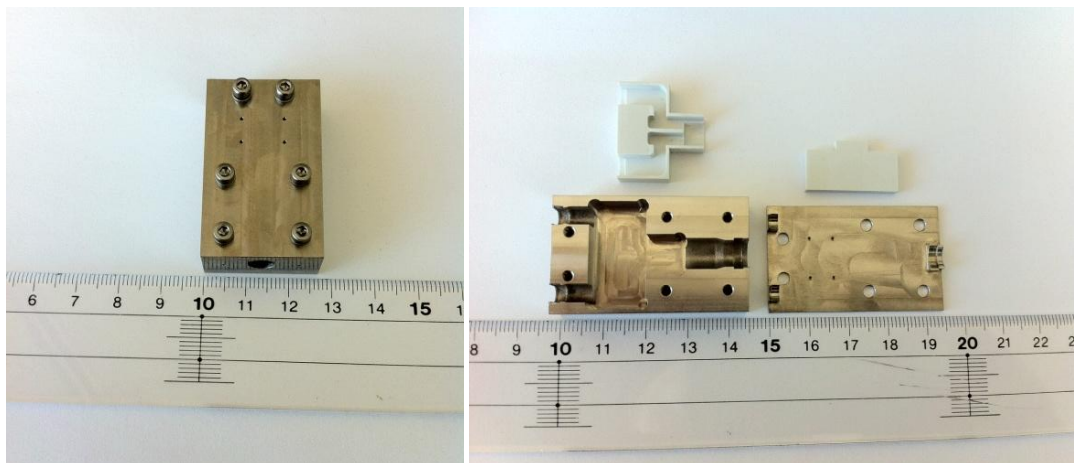*Figure 43: Technical drawing of the junction box showing its components.*

Figure 44: Photos of the assembled prototype junction box. The dimensions are in centimeters. The material of the junction box base and lid is stainless steel 316L and of the ceramics is aluminum nitride.

Appendix C: Power balance calculations

The relations between conducted power $P_{i \to j}$ and temperature difference $T_i - T_j$ are linear, characterized by overall heat transfer coefficients $U_{i \to j}$

$$P_{1 \to 1'} = U_{1 \to 1'}(T_1 - T_1'), \quad P_{2 \to 2'} = U_{2 \to 2'}(T_2 - T_2'), \tag{C.1}$$

$$P_{1' \to sur} = U_{1' \to sur}(T_1' - T_{sur}), \quad P_{2' \to sur} = U_{2' \to sur}(T_2' - T_{sur}), \tag{C.2}$$

$$P_{1' \to 2'} = U_{1' \to 2'}(T_1' - T_2'). \tag{C.3}$$

Because only the temperature difference is measured the power balances of equations (5.6-5.8) and the conduction equations (C.1-C.3) are subtracted to yield the net power balances

$$P_{1 \to 1'} - P_{2 \to 2'} = (\alpha_1 - \alpha_2)pS - \sigma S(\varepsilon_1 T_1^4 - \varepsilon_2 T_2^4 - (\varepsilon_1 - \varepsilon_2)T_{sur}^4) - \rho cV \frac{d(T_1 - T_2)}{dt}, \tag{C.4}$$

$$P_{1 \to 1'} - P_{2 \to 2'} = P_{1' \to sur} - P_{2' \to sur} + 2P_{1' \to 2'}, \tag{C.5}$$

$$P_{1 \to 1'} - P_{2 \to 2'} = U_{1 \to 1'}(T_1 - T_1') - U_{2 \to 2'}(T_2 - T_2'), \tag{C.6}$$

$$P_{1' \to sur} - P_{2' \to sur} = U_{1' \to sur}(T_1' - T_{sur}) - U_{2' \to sur}(T_2' - T_{sur}), \tag{C.7}$$

$$P_{1' \to 2'} = U_{1' \to 2'}(T_1' - T_2'). \tag{C.8}$$

Combining all equations and substituting the equivalent quantities (5.9-5.11) gives

$$\Delta P = \alpha pS - \varepsilon \sigma S(T_1 + T_2)(T_1^2 + T_2^2)\Delta T - \rho cV \frac{d\Delta T}{dt}, \tag{C.9}$$

$$\Delta P = \Delta P' + 2P_{1' \to 2'}, \tag{C.10}$$

$$\Delta P = U^*(\Delta T - \Delta T'), \tag{C.11}$$

$$\Delta P' = U'\Delta T', \tag{C.12}$$

$$P_{1' \to 2'} = U_{1' \to 2'}\Delta T'. \tag{C.13}$$

Substitution now yields a relation between the difference in incoming power ΔP between the two bodies and the difference in temperature ΔT

$$\Delta P = (U' + 2U_{1' \to 2'})\Delta T', \tag{C.14}$$

$$\Delta P = (U' + 2U_{1' \to 2'})\left(\Delta T - \frac{\Delta P}{U^*}\right), \tag{C.15}$$

$$\Delta P = \frac{U^*(U' + 2U_{1' \to 2'})}{U^* + U' + 2U_{1' \to 2'}}\Delta T. \tag{C.16}$$

The other three unknown variables can be calculated with the following equations

$$T_1' = \frac{P_{1\to1'}(U' + U_{1'\to2'}) + P_{2\to2'}U_{1'\to2'}}{U'(U' + 2U_{1'\to2'})} + T_{sur},$$ (A.17)

$$T_2' = \frac{P_{1\to1'}U_{1'\to2'} + P_{2\to2'}(U' + U_{1'\to2'})}{U'(U' + 2U_{1'\to2'})} + T_{sur},$$ (A.18)

$$T_2 = \frac{(P_{1\to1'}^2 - P_{2\to2'}^2)U_{1'\to2'} + P_{2\to2'}U'(U' + 2U_{1'\to2'})(T_1 - T_{sur})}{P_{1\to1'}U'(U' + 2U_{1'\to2'})} + T_{sur}.$$ (A.19)

Appendix D: Specifications of the proposed microwave detector

Specification	Symbol	Value	
Internal thermal conductivity	k_{int}	390 W/mK	
Density of body	ρ	8960 kg/m^3	
Equivalent emissivity	ε	0.90	
Absorption coefficient difference	α	0.80	
Neutron power density	n	0.4 W/cm^3	
Volume of body	V	579 mm^3	
Absorbing surface of body	S	48 mm^2	
Characteristic length	L_c	12 mm	
Overall heat transfer coefficient	U	0.063 W/K	
Equivalent heat transfer coefficient	U_{eq}	0.072 W/K	
Difference in Seebeck coefficients	$S_{Cr} - S_{Al}$	41 µV/°C	
Transient sensitivity in temperature	$d\Delta T/dt/p$	1.93·10^{-5} Km^2/J	
Transient sensitivity in voltage	$d\Delta V/dt/p$	7.91·10^{-10} Vm^2/J	
Steady state sensitivity in temperature	$\Delta T/p$	5.65·10^{-4} Km^2/W	
Steady state sensitivity in voltage	$\Delta V/p$	2.32·10^{-8} Vm^2/W	
Maximum transient Biot number	Bi	0.15	
Maximum steady state Biot number	Bi	0.08	
Characteristic response time	τ	1.3 s	
Temperature range	T	100 °C	816 °C
Specific heat capacity	c	395 J/kgK	463 J/kgK
Modulus of elasticity	E	199 GPa	129 GPa
Force stainless steel bolt	F	601 N	340 N
Force alumina bolt and copper foil	F	235 N	217 N

Appendix E: Error analysis summary

Bolt type	Alumina M3x7						Stainless steel M2x8					
Isothermal block type	None			Aluminum nitride / Copper			None			Aluminum nitride / Copper		
Error source \ Error mode	Maximum power density — Conduction term	Maximum power density — Transient term	Minimum power density	Maximum power density — Conduction term	Maximum power density — Transient term	Minimum power density	Maximum power density — Conduction term	Maximum power density — Transient term	Minimum power density	Maximum power density — Conduction term	Maximum power density — Transient term	Minimum power density
Radiation	7 %	-	-	7 %	-	-	7 %	-	-	7 %	-	-
Non-constant conduction	4 %	-	-	4 %	-	-	28 %	-	-	28 %	-	-
Maximum radiation and conduction error	7%	-	-	7%	-	-	28 %	-	-	28 %	-	-
Non-constant Seebeck coefficient	3 %	3 %	3 %	3 %	3 %	3 %	3 %	3 %	3 %	3 %	3 %	3 %
Non-zero junction temperature difference	8 %	8 %	8 %	0 %	0 %	0 %	8 %	8 %	8 %	0 %	0 %	0 %
Non-constant heat capacity	-	17 %	-	-	17 %	-	-	17 %	-	-	17 %	-
Non-steady state	-	-	13 %	-	-	13 %	-	-	13 %	-	-	13 %
Electromagnetic interference	-	-	3 %	-	-	3 %	-	-	3 %	-	-	3 %
Total error	18 %	28 %	27 %	10 %	20 %	19 %	39 %	28 %	27 %	31 %	20 %	19 %
Acceptable error	yes	no	no	yes	yes	yes	no	no	no	no	yes	yes
Overall acceptable error	no			yes			no			no		